The polygenetic Kahouanne Seamounts in the Northern Lesser Antilles Island Arc: Evidence for large-scale volcanic island subsidence

Carey, S.[1*], Sparks, R.S.J.[2], Tucker, M.E.[2], Li, T. Robinson, L.[2], Watt, S.F.L.[3], Gee, M.[3], Hastie, A.[3], Barfod, D.N.[4], Stinton, A.[5], Leng, M.[6], Raineault, N.[7], and Ballard, R.D.[7]

*Corresponding author scarey@uri.edu

1. Graduate School of Oceanography, University of Rhode Island, Narragansett, R.I. 02882
2. School of Earth Sciences, University of Bristol, Clifton BS8 1RJ, Bristol, UK
3. School of Geography, Earth and Environmental Sciences, University of Birmingham, Edgbaston Birmingham, B15 2TT, UK
4. NERC Argon Isotope Facility, SUERC, Scottish Ent. Tech. Park, Rankine Ave., East Kilbride, G750QF, UK
5. Montserrat Volcano Observatory, PO Box 316, Flemmings, MSR 1110, Montserrat
6. British Geological Survey, Environmental Science Centre, Keyworth, Nottigham NG12 5GG, UK
7. Ocean Exploration Trust, Graduate School of Oceanography, University of Rhode Island, Narragansett, R.I. 02882

Submitted to Marine Geology, 2019

Abstract

Remotely operated vehicle (ROV) explorations of the Kahouanne seamounts, located 25 km SE of Montserrat in the northern Lesser Antilles island arc, have discovered the occurrence of honeycomb-scalloped erosional features on volcanic and limestone outcrops at depths of up to 600 meters below sea level (mbsl). These features, combined with the flat-topped morphology of the seamounts, the occurrence of shallow-water carbonates (rhodoliths, benthic foraminifera), and the presence of oxidized, highly-vesicular volcanic fragments, suggest that the seamounts were once subaerial islands and have subsequently subsided to their present depth. The subsidence is likely to have been in response to a combination of 1) graben development southeast of the island of Montserrat where faulting and extension are driven by the accommodation of slip convergence associated with oblique subduction along the Lesser Antilles volcanic arc and 2) regional subsidence inferred from studies of nearby carbonate platforms. $^{40}Ar/^{39}Ar$ dating of basalt/andesite lavas from the central seamount indicates active volcanism around 5.4 Ma. Shallow-water carbonates recovered from an apparent wave-cut terrace at ~600 mbsl in the same area, were deposited approximately 3 Ma, based on Sr-isotope stratigraphy, indicating significant subsidence of the complex since that time. The total subsidence is in line with displacements in the Kahouanne valley graben and regional subsidence rates inferred from carbonate platform depths around the islands of Guadeloupe and Martinique, implying that intra-arc subsidence has been a significant process shaping the present bathymetry and topography of this island arc.

1. Introduction

The northern part of the Lesser Antilles subduction zone is a complex area consisting of an older eastern line of uplifted limestone platforms (Limestone Caribees) and a narrow western segment of younger volcanic centers (Volcanic Caribees, Martin-Kaye, 1969; Bouysse et al., 1990). Recent multibeam and seismic surveys reveal the development of extensive fault systems with associated intra-arc graben formation in the area southeast of the island of Montserrat (Feuillet et al., 2010) and further south around Guadeloupe (Feuillet et al., 2002). Such features are common in other arc systems (Yamaji, 1990; Ingersoll, 2011) and in some cases are part of an evolutionary sequence involving successive splitting of arc platforms in response to marginal basin formation (Karig, 1971). Regardless of their origin, intra-arc basin formation in subduction zones leads to important sedimentary depo-centers where thick accumulations of volcaniclastic and biogenic sediments build up rapidly owing to the proximity of volcanic and associated carbonate platform sources (Clift et al., 1994; Carey and Schneider, 2011; Carey, 2000; Trofimovs et al., 2010). For example, IODP drilling and seismic surveys to the southeast of Montserrat have identified several hundred meters of interbedded volcaniclastic and hemipelagic deposits derived from a variety of mass-wasting and eruption-related processes that have shaped the Centre Hills and Soufrière Hills volcanoes on Montserrat (Lebas et al., 2011; Watt et al., 2012; LeFriant et al., 2015; Coussens et al., 2016) (Fig. 1). Subsidence rates in intra-arc basins are likely to be high and can impact both the distribution and evolution of nearby volcanic centers (Yamaji, 1990; Clift et al., 1994b). In addition, there may be wider scale regional subsidence in rifted arcs related to a variety of possible factors including extension itself, cooling in the forearc, changes in subduction plate coupling, changes in density of the active arc crust related to igneous

differentiation and volcanism, and coseismic deformations associated with megathrust earthquakes (Leclerc and Feuillet, 2019). In the northern Lesser Antilles, there is evidence for the subsidence of marginal reefs surrounding Guadeloupe and Martinique, at rates of decimeters per thousand years (e.g. LeClerc et al., 2014; 2015). There is also evidence for localized uplift along the arc (Leclerc and Feuillet, 2019) including on Montserrat, notably at Roche's Bluff (Harford et al. 2002)

The Kahouanne seamounts lie about 25 km southeast of the island of Montserrat at the eastern side of an asymmetrical graben (Kahouanne Valley), oriented in a NW-SE direction and with greater throw along the western side (LeBas et al., 2011, Fig. 1). A vibracore sample from the crater of the central seamount recovered basaltic rocks (Cassidy et al., 2012), but little is known about the age or evolution of the complex. New multibeam mapping and remotely-operated vehicle (ROV) explorations of the seamounts were carried out during cruise NA037 of the E/V *Nautilus* in 2013 (Carey et al., 2014). Here we report evidence of extensive subsidence of the seamounts, including the first reported occurrence of honeycomb-scalloped erosional features from deep-sea outcrops. We argue that these distinctive features are uniquely the result of salt weathering along rocky coastlines and/or the effects of bioerosion by echinoids in shallow water, creating the ichonofossil *Circolites*. Thus the honeycomb-scalloped structures provide compelling evidence for previous subaerial exposure and coastal erosion. The discovery indicates that part of the Kahouanne seamounts were once volcanic islands, but that they have undergone significant subsidence of at least several hundred meters to their present position. This paper presents the multifaceted evidence for subsidence of the Kahouanne

seamounts and considers possible causes of their subsidence in terms of larger scale tectonics and volcanic arc evolution.

2. Geologic Setting

The Kahouanne seamounts are located in the northern Lesser Antilles arc between the islands of Montserrat and Guadeloupe and lie on the northeastern side of the NW-SE trending Kahouanne Valley (Fig. 1). Montserrat consists of four volcanic centers that decrease in age from the Silver Hills (~2.1 – 1.04 Ma) in the north through the Centre Hills (~1.14 – 0.38 Ma), Soufrière Hills (~0.45 Ma to present) and South Soufrière Hills (0.13-0.12 Ma) in the south (Hatter et al., 2018, Harford et al., 2002). Eruptive products consist of andesitic lava domes, volcaniclastic debris aprons produced by pyroclastic flows and lahars, debris avalanches and lithic- and pumice-rich tephra fall deposits (Hatter et al., 2018, Coussens et al., 2017, Harford et al., 2002). Basaltic and basaltic-andesite lava flows, domes and scoria fall characterize the South Soufrière Hills center (Cassidy et al., 2015, Harford et al., 2002). The Soufrière Hills volcano (SHV) consists of a cluster of four lava domes (Gages, Perches, Galways and Chances Peaks) surrounding the amphitheater-shaped English's Crater open to the east (Wadge et al., 2014). The lava dome formed in the 1995-2010 eruption partially infilled English's Crater.

The Soufrière Hills complex and two uplifted areas to the NW (Garibaldi Hill and St Georges Hill) and to the SE at Roche's Bluff are located within a WNW trending half-graben structure bounded by the Belham Valley and Richmond Hill faults (Fig. 1; Feuillet et al., 2010). The graben extends offshore to the NW to join the Montserrat Havers Fault system. Two former volcanic centers, Havers Volcano seamount and the

island of Redonda, are located WNW and NW of Montserrat on WNW trending fault systems (Fig. 1). To the southeast of Montserrat the Kahouanne valley is identified as a half-graben bounded on the southwest side by the Bouillante-Montserrat Fault System (BMFS) and on the northeast side by a number of smaller normal faults that transect the Kahouanne complex and are antithetic to the major faults of the Bouillante-Montserrat fault system (Fig. 1). Feuillet et al. (2010) attributed the faults and extensional tectonics in this part of the Lesser Antilles to the accommodation of left-lateral motion caused by partitioning of oblique convergence along the arc.

Inferred vertical offsets for some of the sedimentary units that fill the Kahouanne valley on the western side range from <400 m for upper sequences to >1000 m for deeper units based on high-resolution seismic profiles (Feuillet et al., 2010). Sediment thicknesses have previously been mapped throughout the Kahouanne valley using a grid of 2D seismic reflection profiles collected on the JC45/46 research cruise (see Watt et al., 2012, for acquisition details and complete descriptions of interpreted horizons). Watt et al. (2012) identified a fan of volcaniclastic debris east of the Centre Hills volcano, and correlated the base of this fan with the earliest known age of Centre Hills volcanism (current estimates range from 950 ka (Harford et al., 2002) to 1.14 Ma (Hatter et al., 2018)). This horizon can be traced throughout the graben (Fig. 18 in Watt et al., 2012) and shows that 500 m of material has accumulated on the western side of the graben since this time, compared with <200 m on the adjacent platform. Two of the JC45/46 profiles are shown in Fig. 2 (line locations in Fig. 1), and highlight two major debris avalanche deposits derived from Montserrat, Deposits 2 and 8 (Le Friant et al., 2004; Watt et al., 2012), above the base-Centre-Hills horizon. Smaller volumes, older debris avalanche

deposits may also have been derived from the seamounts themselves (Lebas et al., 2011). These large landslide deposits are bounded by parallel-bedded sediments that fill the Kahouanne valley. In both JC45-M and JC45-3 these sediments are seen to lap up against the sides of the Kahouanne seamounts. The profiles show that the western flanks of the seamounts lie well below the base-Centre-Hills horizon, and that the equivalent horizon is buried to a depth of at least 500 m in the central part of the Kahouanne valley (Fig. 2). We have mapped this surface in the two profiles as the top-Kahouanne horizon. The age of this horizon is discussed further in Section 5.1. The seismic reflection profiles highlight several sub-parallel dipping reflections within the Kahouanne seamounts, defining individual packages of reflectors consistent with multi-stage growth of the structures. On JC45-3, sub-horizontal, irregular reflections are present, potentially defining a base to the Kahouanne seamounts and indicating different characteristics to the valley-filling sediments beneath the top-Kahouanne horizon. High resolution versions of seismic lines JC45-M and JC45-3 are presented in figure 1 of the supplemental data.

The seamounts comprise three main edifices, broadly aligned parallel to the BMFS trend, over a distance of 15 km. The largest, central seamount (B) rises from an exposed base at 1100 m below sea level to a summit at slightly over 500 m water depth. Given the burial of the lower flanks (Fig. 2), this edifice has a height well in excess of 1 km and a basal diameter of approximately 8 km. The surface morphology and structural relationships evident in seismic reflection profiles and multiple dipping reflectors suggest that the complex represents a long-lived polygenetic volcanic system.

3. Methods

Multibeam mapping of the Kahouanne's seamounts was carried out using a hull-mounted Kongsberg EM302, 30 kHz system on the E/V *Nautilus* during cruise NA037. At the water depths of the Kahouanne seamounts (550-700 m) the horizontal resolution is approximately 10 m. A Kongsberg Seatex Seapath 330+ was used for navigation and as a vessel motion reference unit (MRU). Sippican MK21 expendable bathythermographs (XBTs) were used for sound velocity corrections. Data were processed in Caris HIPS and SIPs.

Remotely-operated vehicle (ROV) explorations were carried out using the two-vehicle *Argus*/*Hercules* system on the E/V *Nautilus* during the same cruise. Both *Argus* and *Hercules* are equipped with high-definition video cameras. A single dive on Oct. 27-28, 2013 (H1311) was devoted to the Kahouanne seamounts with a duration of 17 hours. Eight geological samples were recovered using the *Hercules* manipulator arm during the dive (Table 1).

Thin-sections were made of a subset of the collected samples and examined with a petrographic microscope for the identification of volcanic lithologies and fauna. Major and trace element abundances of two lava samples (both from the summit region of the central seamount) were analysed using a JY Horiba Ultima 2 inductively coupled plasma optical emission spectrometer (ICP-OES) and a Thermo X7 series inductively coupled plasma mass spectrometer (ICP-MS) at Cardiff University, United Kingdom. Powdered samples were prepared for analysis by lithium metaborate fusion followed by acid digestion. To obtain major element abundances approximately 20 ml of the sample solution was run on the ICP-OES. For rare earth element (REE) and trace element

abundances 1 ml of the solution was added to 1 ml of In and T1 and 8 ml of 2 % HNO_3 and analysed on the ICP-MS. To test the accuracy and precision of the ICP-OES/MS analysis JB1b (basaltic-andesite) was used as a reference material. Accuracy was ± 4% for the majority of the elements. The precision of the elemental ratios, excluding Cu and Ga, is better than 4% (RSD). Details of the sample preparation procedure, along with the chemical analyses, are presented in the supplemental procedures and data section.

The same two samples were selected for $^{40}Ar/^{39}Ar$ dating of feldspar phenocrysts. Samples were crushed to 250-500 micron size fraction and feldspars were separated using standard techniques. Feldspars were subsequently acid leached in 3N nitric acid to remove alteration products and hand-picked to produce a purified separate. Samples and neutron flux monitors were packaged in copper foil and stacked in quartz tubes with the relative positions of packets precisely measured for later reconstruction of neutron flux gradients. The sample package was irradiated in the Oregon State University reactor, Cd-shielded facility. Alder Creek sanidine (1.1891±0.0008 (1σ) Ma, Niespolo et al. 2016) was used to monitor ^{39}Ar production and establish neutron flux values (J) for the samples. Gas was extracted from samples via step-heating using a mid-infrared (10.6 μm) CO_2 laser with a non-gaussian, uniform energy profile and a 3.5 mm beam diameter rastered over a sample well. The samples were housed in a doubly-pumped ZnS-window laser cell and loaded into a copper planchette containing nine 1 cm^2 square wells, holding ~50 mg per aliquot. Liberated argon was purified of active gases, e.g., CO_2, H_2O, H_2, N_2 and CH_4, using three Zr-Al getters; one at 16°C and two at 400°C. Data were collected on a GVi Instruments ARGUS V multi-collector mass spectrometer using a variable sensitivity faraday collector array in static collection (non-peak hopping) mode (Mark et

al., 2009). Time-intensity data are regressed to inlet time with second-order polynomial fits to the data. The average total system blank for laser extractions, measured between each sample run, was $2.2\pm0.5\times10^{-15}$ mol ^{40}Ar, $1.5\pm0.4\times10^{-17}$ mol ^{39}Ar, $1.0\pm0.3\times10^{-17}$ mol ^{36}Ar. Mass discrimination was monitored on a daily basis, between and within sample runs by analysis of an air standard aliquot delivered by an automated pipette system (see raw data for D values applied to individual steps). All blank, interference and mass discrimination calculations were performed with the MassSpec software package (MassSpec, version 8.16, authored by Al Deino, Berkeley Geochronology Center). A step-heating analysis was considered to yield a plateau if 1) the ages of 3 or more consecutive steps representing >50% of the ^{39}Ar release were indistinguishable at 2σ uncertainty (neglecting uncertainty in J); 2)the steps included in the plateau yield a trapped component composition, $^{40}Ar/^{36}Ar_i$, indistinguishable from atmospheric argon on an inverse isochron plot and 3) the inverse isochron age was indistinguishable from the plateau age. The two samples presented here conform to these criteria. Inverse-variance-weighted plateau ages, or composite plateau ages for replicated samples, were chosen as the best estimates of the timing of emplacement. The composite age was calculated using all of the accepted plateau steps (n=12) from the two individual analyses.

In addition, three carbonate samples were selected for strontium isotope seawater-age stratigraphic determinations. Isotopic ratios were measured on a Thermo-Finnigan Triton thermal ionization mass spectrometer following the established protocols in the Bristol Isotope Group at the University of Bristol (Lewis et al., 2014). Samples and $TaCl_5$ activators (Birck, 1986) were loaded onto single rhenium filaments. ^{85}Rb was monitored in order to correct the interference of ^{87}Rb on ^{87}Sr using a $^{85}Rb/^{87}Rb$ ratio of 2.59265.

Amplifier efficiency and mass-bias for the mass spectrometer were both corrected in a peak jumping mode (Heuser et al., 2002) with a 4.194 s integration time per cycle and 200 cycles per block. The long-term reproducibility of $^{87}Sr/^{86}Sr$ for NIST SRM 987 isotope standard treated with column chemistry was 0.710242 ± 0.000010 (2 SD, n = 5). Details of the sample preparation are given in the supplemental procedures and data section.

To check for any alteration of the carbonate samples used for Sr analysis, stable carbon and oxygen isotope analysis was undertaken. Samples were ground in agate and an equivalent of 10 mg of carbonate was reacted with anhydrous phosphoric acid in vacuo for 72 hours at a constant 25°C (Ca and Mg carbonates including dolomite should react within this time). The CO_2 liberated was separated from water vapour under vacuum and collected for analysis. Measurements were made on a VG Optima mass spectrometer at BGS Keyworth. Overall analytical reproducibility for these samples is normally better than 0.2‰ for $\delta^{13}C$ and $\delta^{18}O$ (2s). Isotope values ($\delta^{13}C$, $\delta^{18}O$) are reported as per mil (‰) deviations of the isotopic ratios ($^{13}C/^{12}C$, $^{18}O/^{16}O$) calculated to the VPDB scale using a within-run laboratory standard calibrated against NBS standards. The results, given in Table 2, show normal-marine values for both $\delta^{13}C$ and $\delta^{18}O$ (discussed further in Section 4.3.2). These indicate no significant alteration, and thus that the samples should provide reliable Sr isotope signatures.

4. Results

4.1 Morphology of the Kahouanne seamounts

The Kahouanne complex can be divided into three morphological regions (Fig. 3). At the southeast edge of the complex is an irregular circular structure about 3.5 km in diameter comprising multiple domed rock masses but without any prominent summit craters. To the NW, between this southernmost seamount and the large, central seamount, is a small cone topped by a circular volcanic crater about 0.5 km in diameter at a depth of 800 meters below sea level (mbsl), here referred to as seamount C following after the designations of LeBas et al. (2011) for the other seamounts. This lies close to the oblate-shaped central seamount (B) that contains a larger circular depression 1.5 km in diameter and an extensive flat terrace at a depth of 590 meters on its eastern and northeastern side (Fig. 3). Within the depression are six circular dome or knoll-like structures that rise roughly to the same depth as the eastern terrace. On the southeast corner of the depression is a prominent, steep-sided outcrop that rises to a depth of 518 m, the shallowest point on the central seamount (Fig. 4). This feature could be either the remnant of a dome or the remaining segment of a pre-existing crater wall. In the northwest and southeast, the depression is intersected by several prominent south-facing scarps that trend NW to SE, roughly parallel to the trend of the BMFS. The maximum offset measured at the southern margin of the depression is 35 meters (Fig. 3). A horseshoe-shaped feature on the northwest corner of the central seamount appears to be the scar from a small lateral collapse directed to the northwest, although the bounding sides of the scar are oriented in the same direction as the other normal faults on the seamount. In deeper water (~1095 m) to the northwest, there are numerous isolated blocks that are thought to be a debris field associated with this collapse (Fig. 3), previously identified as Deposit 12 in Lebas et al. (2011). Radial ridges are also present

on the northern and eastern flanks of the seamount, separated by broad gullies, and possibly representing other shallow-seated erosional features.

A third, flat-topped seamount (A) lies to the north of the central complex and consists of an irregularly-shaped area with multiple fault scarps along its western and southwestern side (Figs. 3 and 4). The flat summit of this area is similar to, or just slightly deeper than, the flat eastern terrace of the central seamount. Offsets on the NW-SE oriented fault scarps are up to 60 meters. In the central western part of this seamount there are several small dome-like structures that rise up to 80 meters above the surrounding seafloor (Fig. 4). The eastern flank is marked by scalloped features that may be the source of a flank failure. The overall morphology of the seamount is more irregular than that of the elliptical central seamount, and the structure appears to be more degraded and eroded. Seismic reflection profiles through the margins of the seamounts suggest that the northern seamount is older than the central one, and that overlapping units of the two centers form a ridge between them (Figs. 1 and 2).

4.2 ROV Explorations

Part of the Kahouanne seamount complex was explored using the remotely operated vehicles *Hercules* and *Argus* during cruise NA037 of the E/V *Nautilus*. Dive H1311 began in the southern part of the complex in the area of seamount C (Fig. 4b with dive track). The crater floor is almost completely covered by fine-grained hemipelagic sediment. Exposures along the crater rim at 800 m depth are moderately indurated and consist of coarse volcaniclastic deposits with individual clasts up to 20 cm in diameter. Some of the clasts in these poorly-sorted deposits are rounded and coated with

manganese crusts (Fig. 5a). Crude bedding was observed in some areas along lateral transects of the deposits. Other massive outcrops in this area have smoothed and incised surfaces that are similar to sculptured subaqueous lavas described by Paduan et al. (2009) on the submerged San Juan bank off the California coast (Fig. 5b).

On the southeast side of the central seamount B a field of meter-sized boulders and scattered outcrops exhibit distinctive pock-marked and sculpted surfaces that strongly resemble honeycomb weathering and bioerosion features observed in subaerial to shallow subtidal coastal environments (e.g. Mustoe, 1982; Kazmer et al., 2015; Zwalinska and Dabski, 2012). Individual pock-marks range in size from several to tens of centimeters in diameter and in some cases are aligned in a linear fashion (Fig. 6a,b,c). Samples collected from the boulders consist of altered plagioclase- and hornblende-phyric andesite, commonly with a thin manganese coating. In the same general area there are horizontally-bedded outcrops of carbonate-rich sediments that are a mixture of coarse coralline algal fragments, rhodoliths and fine-grained sediment, and these show features which are likely the effects of bioerosion by echinoids and sponges. Farther along towards the circular crater, parts of the seafloor are covered with coarse, broken, branching coral debris with some manganese coating, clearly relict (i.e. sub-recent). No live corals were observed in this area. The pieces of branching coral are likely derived from living coral colonies found farther upslope.

Within the circular crater of seamount B a prominent spire was explored from its base to the peak (Fig. 4). At the base, large talus blocks with common honeycomb features are partially covered with fine-grained carbonate sediment. Outcrops of altered basalt/andesite show persistent sculpting and honeycomb features on the steep-sided spire

up to the flat-topped summit at 500 meters where numerous modern deep-sea corals are growing (Fig. 6d.).

From the base of the spire towards the north, a flat area of fine-grained unconsolidated sediment with scattered outcrops of pock-marked and sculptured andesite with manganese and carbonate crusts extends for several tens of meters. In the center of the crater a cluster of domes (Fig. 4b) exhibit similar outcrops of highly sculpted and honeycombed lava protruding through gray hemipelagic sediment (Fig. 7a). Some outcrops are extensively fractured and faulted resulting in an unusual rectangular surface pattern (Fig.7b). In the area of the northernmost dome the seafloor has abundant open bivalve shells and coral fragments, some apparently discolored by a manganese coating, but no live specimens were observed (Fig. 7c).

4.3 Lithology and dating of collected samples

Recovered samples from ROV dive H1311 consist of both volcanic and biogenic material. In view of the highly indurated nature of most outcrops, samples were typically collected from loose pieces found as close as possible to the base of the deposits.

4.3.1. Volcanics

Several volcanic rock samples (NA037-049, 050, 051, 052, 055 and 058) have been examined in thin-section, and two of these (052 and 055) have been analyzed chemically and dated through $^{40}Ar/^{39}Ar$ analyses.

Sample NA037-050 from the rim of the southern crater in seamount C (Fig. 4b) consists of angular to subrounded, highly-vesicular fragments of altered volcanic rock with a red-oxidized color (Fig. 8a). The fragments are indurated being bound together by an isopachous quartz cement. Individual fragments range from dense plagioclase-phyric

andesite lava to highly vesicular scoria (Fig. 8b) and vary in size from a few hundred microns to several millimeters. A remarkable feature of this heterogeneous volcaniclastic sandstone is the presence of small ostracod shells (200 microns in length) that occupy some of the interstitial pore spaces. Clearly, the ostracods inhabited cavities remaining after quartz cementation (Fig. 8c), although some are filled by fine-grained calcite sediment. The ostracods have then been cemented by a syntaxial fibrous calcite overgrowth, typical for ostracods, and the remaining pore-space filled by sparry calcite (Fig. 8c). The ostracods appear to be smooth shelled forms. Ostracods can occur in freshwater, brackish, and marine environments, shallow to deep, including volcanic crater lakes (e.g. Gouramanis et al., 2010) and sediment-interstitial forms are common. Although smooth-shelled ostracods are more typical of freshwater lakes (e.g. Pérez et al., 2010) but can occur elsewhere. With their extremely small size and occurrence on an isolated seamount, they are probably more likely to be marine (Robin Smith pers. comm.). Unfortunately, being only seen in thin-section, an unambiguous determination of the specific ostracod species is impossible.

Sample NA037-049 was collected nearby sample 050, in the western part of southern seamount C, whereas NA037-051 was collected on a ridge near the NW edge of the crater (Fig. 4b). Both are highly porphyritic greenish-grey dense lavas dominated by plagioclase, with clinopyroxene and olivine in sample 51, and more common orthopyroxene in sample 49. They also show extensive secondary mineralization of clay minerals and calcite in vesicle and fracture spaces, and Fe-oxyhydroxide alteration of pyroxenes. The mineral assemblage suggests a basaltic-andesite bulk composition, and the absence of amphibole contrasts with samples from seamount B.

Samples NA037-052, 055 and 058 are lava blocks collected from the central seamount B. Sample 052 is a dense clast from a honeycombed block at the southern edge of the spire on the eastern crater rim, whereas 055 was collected from the small dome located in the southern part of the seamount's B crater (Fig. 4b), and 058 was collected from a smaller dome in the northern part of the central crater (Fig. 8d). All three samples are highly porphyritic (50 vol.% for 052 and 45 vol.% for 055) and dominated by plagioclase and amphibole phenocrysts. Sample 052 is highly altered, with extensive calcite mineralization within the groundmass and affecting plagioclase phenocrysts. Plagioclase is the most abundant phenocryst phase, followed by amphibole and orthopyroxene. Amphiboles are present as pseudomorphs, entirely replaced by a largely opaque alteration assemblage. Sample 055 is much less altered and has a phenocryst assemblage of plagioclase and amphibole with minor olivine. Amphibole phenocrysts are well preserved, up to 4 mm across. Sample 058 is petrographically similar to 052, being dominated by plagioclase and hornblende. The groundmass is extensively altered to a clay mineral assemblage, but there is fresh hornblende with oxidized reaction rims.

The varied mineralogy both within the seamount B samples, and between this seamount and seamount C, is consistent with a long-lived magma system erupting a variety of compositions. Alteration is apparent in bulk chemical analyses of samples 052 and 055 (Table 1 in supplemental data). Both have high LOI values (11 wt% for 052 and 9 wt% for 055), and comparison with major-element compositional trends of volcanic rocks from Montserrat (Zellmer et al., 2003; Cassidy et al., 2012) suggest relatively elevated Al, Na and K contents, low Fe and Ti, and variable Ca and Mg contents. The unusually high CaO content in 052 (19 wt% for recalculated anhydrous compositions), in

addition to the anomalously low silica content (43 wt%) likely reflects the calcite mineralization observed in thin-section. The broad pattern of major element compositions and phenocryst assemblages suggests a primary basaltic-andesite or andesite composition for 052. The CaO content of sample 055 (8.7 wt%, anhydrous) is normal for Lesser Antilles basalts, whereas the silica content is low (45 wt%,anhydrous). The high MgO content (10 wt%, anhydrous), high Cr (113 ppm) and Ni (297 ppm), and the abundance of amphibole and presence of olivine suggest a primitive basalt composition. Rare Earth and incompatible trace element compositions of these rocks are similar to rocks from the South Soufrière Hills, Montserrat (Cassidy et al., 2012).

Feldspar phenocrysts from NA037-055 and NA037-052 were used for $^{40}Ar/^{39}Ar$ dating. Plateau ages were indistinguishable for the two samples yielding 5.37±0.56 Ma for NA037-052 and 5.38±0.24 Ma for NA037-055 (Table 3, Fig. 9).

4.3.2 Carbonates

In general, carbonate outcrops on the seamounts were sparse due to the extensive cover of unconsolidated hemipelagic sediment. Scattered outcrops were typically found close to the dome structures on seamount B's crater floor and in the vicinity of the spire on the southeast corner. Three carbonate samples were recovered of two distinctively different types of carbonate, one of shallow and one of deep-water facies. Sample N037-053, collected on the relatively flat terrace near the spire, is a coarse-grained carbonate (Fig.10a) that contains shallow-water foraminifera, *Amphistegina* and *Peneroplis*, which are typical of tropical lagoons and reefal environments (Fig.10b). Also present are calcareous red algae, in the form of rhodoliths, which also form in shallow to moderate water depth under agitated conditions (Marack, 1999; Foster et al., 2013; Rebelo et al.,

2015). In addition, there are ostracods, fragments of echinoids, and pieces of gastropod and bivalve (Fig. 10c). There are few planktic forams and no lithic/volcanic grains. This largely shallow-water limestone was originally quite porous with cavities up to 10 mm between/within bioclasts, and borings in rhodoliths probably formed by sponges. Cements have grown syntaxially on echinoid, foram and ostracod grains (Fig. 10d). Cavities are lined by an isopachous calcite cement and then later filled by pelagic sediment, with 2 generations being present. Planktic forams occur within these sediments. The fully-cemented limestone was later bored, with the organisms cutting through the earlier isopachous cement and pelagic sediment, and the latest borings are filled by sediment containing lithic/volcanic grains. The upper surface of this sample is highly corroded/bioeroded, with some brownish clasts, probably phosphatic, incorporated, and it is covered with a phosphatic Fe-Mn crust. The surface of the outcrop is again sculpted with scoop-scallop shapes with narrow ridges between, on the scale of 5-10 cm, but less regular than the patterns developed on the andesite (Figs. 6a, c).

Sample NA037-057, collected near the northern domes in the central crater of seamount B (Fig. 4b), is a pelagic limestone with planktic foraminifera and fragments of deep-water coral, with few lithic grains/crystals (Fig. 11a,b). The outcrop appears to have been highly corroded and bioeroded, and the rocky seafloor here is being buried by brown-grey hemipelagic mud. The limestone with corals has been extensively bored by clionid sponges and probably some other organisms (polychaetes and bacteria). Sponge spicules are present in some of the more recent borings (Fig. 11c,d). It appears that there were three phases of boring in the history of the sediment: the corals were themselves bored before being buried by pelagic mud, which also filled the borings; the sediment

was then cemented (by very fine-grained calcite) and after a second phase of sponge boring, the cavities were lined with a thin Fe-Mn crust, but otherwise are still open; finally, a more recent phase shows walls of the borings that are still fresh (Fig. 11d). There is a suggestion of some dissolution of the sediment/limestone as shown by cavities with unusual shapes (remnant crystal or foraminifera outlines). Sample NA037-047 is similar to NA037-057 in being a pelagic limestone with fragments of deeper-water coral. Planktic forams are numerous along with thin-shelled bivalves and echinoderm debris. This carbonate has also been bored by sponges and coated with a phosphatic-Fe-Mn crust. This rock was collected from seamount C (Fig. 4) at a depth of 885 m.

The $\delta^{13}C$ values from all carbonate samples are within a relatively small range (+1.39 to +2.52 ‰; Fig. 12; Table 2) and these are within the typical range of most modern and ancient marine carbonates (Tucker & Wright, 1990; Swart, 2015). The $\delta^{18}O$ data on the other hand are interesting in that they fall into 2 groups: the shallower-water sample (NA037-053) has low positive $\delta^{18}O$ (average 1.9 ‰) compared to the two more positive deeper-water limestones (NA037-047 and NA037-057; average 3.6 ‰). This difference is likely to be the result of temperature, the warmer water of the shallow-water sediment relative to the cooler water of the pelagic carbonate, deposited several 100 m deeper. Caribbean seawater temperature is 28-25^{o}C from the surface to ~100 m depth, and then it decreases to around 10 ^{o}C by 400 m water depth (Kameo et al., 2004). Thus, a different $\delta^{18}O$ signature can be expected, a few per mil more positive, for the deeper water carbonates.

Ages of the three carbonate samples have been estimated based on strontium isotopic ratios in comparison with the global seawater strontium isotope curve (Table 4) and data

from Neogene carbonates (e.g. Farrell et al., 1995; Howarth and McArthur, 1997 and the LOWESS 5 fit (09/04/2013 database); McArthur et al., 2006). Of 6 analyses from the shallow-water carbonate sample (NA037-053), 5 give very similar $^{87}Sr/^{86}Sr$ values of 0.709060 (range 0.709058 to 0.709066); these data can be interpreted as indicating an age of approximately 3.2 Ma (LOWESS 2013 database, see Howarth and McArthur, 1997), although the gentle slope of the curve for this time interval means a significant degree of uncertainty (range 2.6 to 3.8 Ma) in the age estimates. The 6th analysis is of internal sediment containing planktic foraminifera filling a cavity within the shallow-water limestone and gives a $^{87}Sr/^{86}Sr$ value of 0.70909, which indicates a date of ~1.9 Ma. This younger age is consistent with the much later input of sediment to the cavities in deeper water during seafloor subsidence. Three analyses from the deeper-water carbonate (NA037-057) give an average $^{87}Sr/^{86}Sr$ value of 0.709164 (range 61-68), indicating a much younger age of ~350 kyr, with a range of 200-400 kyr. Two analyses from the similar pelagic limestone NA037-047 give an average of 0.709155, which suggests an age of 600 kyr.

5. Discussion

Many oceanic seamounts undergo significant amounts of subsidence during their evolution as a result of either large-scale plate tectonic processes or more localized faulting in a variety of volcanic/tectonic settings (Wessel, 1997). A subset may start out as subaerial islands and commonly transform to flat-topped guyots as a result of wave-cut erosion and armoring by coral reef development (Hess, 1946). However, some flat-topped seamounts may be formed entirely in the submarine environment by volcanic

processes (Clague et al., 2000, Chaytor et al., 2007). Paduan et al. (2009) proposed criteria that can be used to assess whether flat-topped seamounts were once subaerial islands. They include the occurrence of beach deposits, distinctive erosional features such as sculpted outcrops, degassed volcanic lavas and pyroclasts, and cooling/alteration patterns. Schwartz et al. (2018) utilized detailed bathymetric analyses of slope maps to identify suspected wave-cut terraces on seamounts from the Galapagos archipelago.

There are several lines of evidence to suggest that the Kahouanne seamounts have undergone significant subsidence and were once subaerial islands. One of the most compelling observations from the ROV explorations is the discovery of outcrops with honeycomb and scalloped erosional features on bedrock at depths of >550 meters (Fig. 6). The honeycomb pattern is a distinctive weathering feature observed in a number of geological locations, but it is best developed in coastal, high intertidal to supratidal environments (Trenhaile, 1987). The shallow cavities, commonly referred to as tafoni, are formed in a variety of rock-types from sedimentary to volcanic (e.g. Zwalinska and Dabski, 2012) and can be developed in both heterogeneous and homogeneous lithologies. Mustoe (1982) proposed that they form by the crystallization of salt solutions deposited as spray in high inter-supra-tidal areas of rocky-cliffed coastlines. Rodriguez-Navarro et al. (1999) reproduced the weathering pattern experimentally through a combination of heterogeneous wind flow and salt crystallization over a homogeneous surface and concluded that evaporative salt crystallization is a key component of this weathering process. To our knowledge there is no submarine weathering process that can produce this type of distinctive honeycomb texture and no examples have been documented from rocks in the deep-marine environment. We suggest that development of such textures is

thus indicative of subaerial exposure, most likely in a high inter-supra-tidal environment where rocks can be repeatedly wetted with saltwater and then dried heterogeneously by the wind. In addition, the abundance of sculpted lava outcrops (Figs. 5,6,7) at various locations on the seamounts also points to erosion in an inter-supratidal setting.

Similar features to this honeycomb pattern can, however, also be produced by boring echinoids, such as *Echinometra* (to give the trace fossil *Circolites*, Asgaard and Bromley, 2008; Santos et al., 2015). Echinoids commonly inhabit the shallow subtidal zone of rocky shorelines, down to depths of several meters, where they feed on algae living either on or within the rocks. They create their 'nests' by rasping the bedrock, to form scoop or scallop-shaped depressions in the rock, typically 8-12 cm across and 4-8 cm deep, with clearly defined ridges around them. Some echinoids extend their 'nest' to create a channel-like feature, reaching 30-50 cm long. The shallow-subtidal-intertidal zone is also a very active zone of bioerosion by several other organisms: chitons, clionid sponges, endolithic bacteria and algae, as well as a site of rock dissolution in the high intertidal-low supratidal zone through microbial activities, repeated exposure-submergence and meteoric influences (producing karren), especially where the bedrock is limestone (Kázmér et al., 2015). Indeed, any rocky shoreline in the tropics is usually intensely bioeroded, as well as being corroded, to give features directly comparable to those observed on the rocky exposures from the deep-sea floor of the Kahouanne seamounts. Additional evidence for subaerial exposure of the complex comes from the oxidized and highly vesicular volcaniclastic deposits found in the southern crater. These features are typically associated with the subaerial eruption of magma.

A second feature of the seamounts that indicates submergence is the general geomorphology of the complex. Two of the major seamounts are characterized by flat terraces that lie at ~600 meters water-depth (Fig. 4). These terraces can also be clearly identified on the basis of very low slopes <1% (Fig. 13 and 14). Neither of the terraces appear to be significantly tilted in any particular direction. They are typical of wave-cut terraces found at some other oceanic seamounts and islands (Paduan et al., 2009; Schwartz et al., 2018; Ricchi et al., 2018). Some terraces at flat-topped seamounts have been interpreted as volcanic constructional features, but in these cases the surfaces show clear evidence of volcanic processes in the form of stacked lava deltas and cones, lava ponding from a central vent, and effusion of low viscosity magma (e.g. Chaytor et al., 2007). These seamounts are commonly associated with hotspot volcanism and dominated by eruption of basaltic magma. In contrast, the Kahouanne seamounts are in an arc environment with basaltic andesite and andesite volcanic products (intermediate compositions can be inferred at Kahouanne from the mineral assemblages of some samples, in addition to the steep-sided dome morphologies, even if alteration prevents a precise bulk-chemical assignation). We did not observe evidence of low-viscosity magmatic constructional features on their terraces and thus favor an erosional, wave-cut origin.

Finally, the lithology of recovered carbonate samples from different locations in the complex and their respective ages support subsidence. The oldest carbonate sample (~3.2 Ma) contains shallow-water foraminifera, *Amphistegina* and *Peneroplis*, which are typical of tropical lagoons and reefal environments. This highly indurated sample also contains calcareous red algae (rhodoliths) that are typically found in high- to moderate-

energy shallow-water settings (Marack, 1999; Foster et al., 2013). The sample was recovered on the wave-cut terrace of the central seamount and represents the remnants of a shallow- to moderate-depth carbonate depositional system that included coralline algae, echinoids, gastropods, bivalves and forams. The relatively complex diagenesis of this sample is also consistent with subsidence: deposition was followed by early cementation and bioerosion; remaining cavities and borings were filled by internal sediment and further cement, with the last generation of fill containing planktic foraminifera, suggesting a location in deeper water. Diagenesis continued into deeper water with further bioerosion and the precipitation of a phosphatic Fe-Mn crust. In contrast, the other two indurated carbonate samples consist of pelagic sediment with planktic foraminifera and fragments of deepwater coral that have been cemented together and subsequently bored by sponges and other organisms. Again several stages of diagenesis are evident, including 3 phases of sponge boring and Fe-Mn encrustation. A similar complex patter of diagenesis as a result of subsidence has been recorded from other seamount carbonates (e.g. Buch et al., 2018). The strontium seawater ages of these samples are significantly younger (~250 and 600 kyr) than the shallow-water carbonate. The observations on these samples indicate formation in deeper water, probably close to their current depth, following subsidence of the seamounts.

5.1 Evolution and Subsidence of the Kahouanne Seamounts

The ages and depths of the volcanic and carbonate samples provide some first-order constraints on the evolution of the Kahouanne seamounts. Volcanism was active about 5.4 Ma ago at the large central seamount B. In the northern part of the Lesser Antilles arc there has been an eastward migration of the arc that started in the late Oligocene-early

Miocene period (Germa et al., 2011). The age of the Kahouanne seamounts shows that the arc was established close to its present location at the beginning of the Pliocene. Kahouanne lies on an arc locus 15 km east of the currently active volcanism on Montserrat, suggesting that it may represent an intermediate stage of volcanism before the current arc position was established at this latitude. The oldest subaerial volcanism on Montserrat is dated at 2.6 Ma (Harford et al., 2002; Hatter et al., 2018). On Guadeloupe, at the southern end of the graben, volcanism extends back to the late Pliocene at ~ 2.8 Ma (Samper et al. 2007). Submarine pyroclastic deposits SE of Montserrat extend to at least 4 Ma (Jutzeler et al., 2016) in IODP core U1396, but the volcanic center for this early volcanism has not been identified.

The shift in location of the northern Lesser Antilles arc has been attributed to a change in subduction geometry caused by the accretion of an oceanic ridge onto the overriding Caribbean plate during the mid-Miocene (Bouysse et al., 1990). Activity at this time in the central Kahouanne seamount likely occurred subaerially on an island that may have been up to 4 km in diameter, based on the maximum extent of its wave-cut platform, and that rose from a seafloor at ~750 m depth, based on seismic reflection data (Fig. 2). This island would have been roughly similar in size to the present island of St. Eustatius in the northern Lesser Antilles.

It is not possible to define precisely when subsidence of the Kahouanne complex began, but at 3.2 Ma there were shallow-water carbonates being deposited either adjacent to the islands or on an insular shelf that had formed by prior subsidence. Within the uncertainties of our dating, 3.2 $\pm$0.5 Ma, sealevel estimates varied from +55 to -75 meters relative to present (Haq et al., 1988). Given the large uncertainties of the dating and

significant variations in sealevel during that period we are not confident in assigning a depth of the shallow carbonate platform at the time subsidence may have begun. That area is currently at a depth of about 600 m. We therefore assume that a total of 600 m of subsidence occurred within the last 3.2 Ma and evaluate the potential processes that led to these vertical movements. Our data imply an average subsidence rate of ~200 m/Ma (+ 50 m/Ma).

The Kahouanne Seamounts lie on the eastern side of a half-graben (Kahouanne Valley) where seismic evidence indicates hundreds of meters of downward displacement of sediment fill on the western side (Fig. 1 and 2). On the eastern side evidence of downward displacement is not as clear and is obscured to some extent by the presence of the seamount complex itself and a fan of volcaniclastic debris sourced from Montserrat (Feuillet et al., 2010; Watt et al., 2012). However, normal faults transect the Kahouanne complex and are antithetic to the major faults of the Bouillante-Montserrat fault system (BMFS), indicating that graben-related subsidence has likely affected the location of the seamounts, but that the total subsidence here is less than that on the western side of the Kahouanne Valley.

To estimate the potential subsidence associated with graben formation we first consider differential sediment accumulation rates between the graben and adjacent areas. From a seismic reflection profile across the Kahouanne Valley north of the seamounts (Feuillet et al., 2010; gwa-039, Fig. 2), two sedimentary units can be defined that show strong thickening within the Kahouanne valley relative to the platform to the NW, which lies north of the Kahouanne seamounts. These units are cut by the main graben faults. The units have a combined thickness of ~150 m (assuming a 1600 m/s seismic velocity) on

the platform, at about 800 m water depth, thickening in the deepest part of the graben to a maximum of 750 m (i.e. a factor of 5 difference in accumulation rate), shown by the base-Unit 2 horizon in Fig. 2. Sedimentation patterns beneath this horizon are obscured by a seafloor multiple (Fig. 2), but the thickening Units 1 and 2 at least suggests graben formation spanning the timescale of their deposition. The base-Unit 2 horizon thus provides a minimum constraint on the timescale of graben subsidence. However, estimating the age of this horizon requires estimates of sedimentation rates.

Sediment accumulation above the base-Centre-Hills horizon (estimated at 950 ka; Harford et al., 2002) was mapped by Watt et al. (2012; cf. their Fig. 18) across the Kahouanne valley, suggesting a maximum thickness of 340 m (again assuming a 1600 m/s velocity) in a cross-valley profile at the Kahouanne seamounts. This thickness reduces to 200 m at the western base of the central Kahouanne seamount, and decreases further to only 50-80 m of sediment on the platform to the NE. The range of these values is in good agreement with the factor of five difference indicated by the gwa-039 profile (Feuillet et al., 2010), suggesting that sediment accumulation patterns mapped by Watt et al. (2012) above the base-Centre-Hills horizon, can also be projected to deeper levels. Using a 950-ka age for the base-Centre-Hills horizon, this approach implies that the base-Unit 2 horizon on gwa-039 (Fig. 2) is at 2.2 Ma in the deepest part of the basin infill, and 1.8 Ma on the platform to the NW, providing an indication of uncertainty and suggesting that graben subsidence has occurred since at least 1.8-2.2 Ma. The same approach implies that the top-Kahouanne horizon in Fig. 2 also lies at ~2 Ma (a younger age is derived from JC45-M than JC45-3 (Fig. 2), which can be seen in the relative differences in thickness between the seafloor-Centre Hills and Centre Hills-Kahouanne packages in the

two profiles. This is arguably attributable to the substantial thickness of Deposits 2 and 8 in the central part of the Kahouanne valley, which may be exaggerating estimates of sedimentation rates above the base-Centre-Hills horizon relative to earlier periods, where thick landslide deposits are not found. Even if volcanism had long-since ceased at the Kahouanne seamounts by ~2 Ma, as implied by our $^{40}Ar/^{39}Ar$ ages, the youngest units on the seamount flanks may be derived from wave-driven erosion of the island edifice during subsidence. The estimated age of the top-Kahouanne horizon is thus consistent with the ~3 Ma Sr-isotope age of shallow carbonate on the seamount, potentially marking the point where the seamounts became fully submerged.

If a higher seismic velocity value were assumed, the thicknesses estimated above would be higher, but the age estimates would not change. If a slightly older age is used for the onset of Centre Hills volcanism (the 1.14 Ma age from Hatter et al., 2018), the estimated base-Unit 2 age becomes 2.1-2.6 Ma. Independent support for the ages derived from the above approach is provided by the age of the Deposit 2 landslide from Montserrat (Fig. 2), which was dated at 130 ka (based on correlated $^{40}Ar/^{39}Ar$ ages) by Cassidy et al. (2015) and is estimated at 140 ka using the above approach (cf. Watt et al., 2012); and by a close similarity to sedimentation rates derived from O-isotope analyses of IODP Site U1394 (Coussens et al., 2016; Fig. 2) since ~350 ka. Thus, we infer that the Kahouanne valley has been forming since at least 2 Ma, and that by this time the seamounts were fully submerged with the wave-cut platforms already formed.

To obtain a minimum estimate of the amount of sediment accumulation since the onset of graben subsidence, we estimate the depth of the base-Unit 2 horizon at the foot of the western flank of the central Kahouanne seamount, relative to the equivalent

horizon on the arc platform to the NE. Incorporating uncertainties in both seismic velocity (1600-2000 m/s) and the age of the base-Unit 2 horizon, we estimate that 225-345 m of excess sediment has accumulated on the eastern side of the Kahouanne valley, at the position of the central seamount. A topographic profile across the Kahouanne valley at this same location illustrates the form of the graben relative to the adjacent seafloor (Fig. 15), and shows that the smooth pattern of deepening from the NE to SW is disrupted by the graben, forming scarps up to 100 m high on the western side. This profile suggests that subsidence at the eastern side of the graben is 250 m, before differential sediment infill is accounted for (Fig. 15). By combining this topographic estimate of subsidence with the estimate of excess sediment accumulation in the graben, we estimate that approximately 500 m of graben-related subsidence has affected the Kahouanne seamounts since ~2 Ma.

The above estimates place the wave-cut platform of the central seamount at about 100 m depth relative to contemporary sea level at ~3 Ma. The shallow-water carbonates observed on the platform are assumed to have formed at sea level to about 50 m depth. Our slightly deeper depth estimate at 3 Ma may potentially be accounted for by eustatic sea-level changes. Nevertheless, our estimates potentially leave 50 meters of subsidence that cannot be accounted for solely by graben formation. There remain some uncertainties in our calculations, and if graben formation started earlier than we estimate above (which we are unable to judge from available seismic reflection data), this may account for the additional subsidence. However, there may be other, regional factors that have also contributed to the subsidence.

Recent studies of drowned carbonate platforms off the islands of Guadeloupe and Martinique have revealed evidence for tectonic subsidence with rates from 300 to 400 m/My, influenced by regional as well as local processes (Leclerc et al., 2014; 2015; Leclerc and Feuillet, 2019). Although the closest of these study sites is about 100 km from the Kahouanne seamounts, the fact that similar subsidence rates are observed between Guadeloupe and Martinique (separated by 170 km) suggests that regional subsidence is indeed impacting a large area of the northern Lesser Antilles, as suggested by Leclerc et al. (2015). A detailed analysis of submerged coral reef complexes from Les Saintes (Guadeloupe) by Leclerc and Feullillet et al. (2019) indicated that their configurations and present depths could only be explained by subsidence and not by westward tilting of the arc platform as evidenced by uplifted carbonate terraces in Grand Terre, Marie Galante and La Desirade. They considered a number of possible mechanisms to explain subsidence of the carbonate platforms including the influence of volcanic activity (magma chamber cooling, loading of volcanic edifices, changes in hydro-static pressures of deep magma chambers), active faulting, and long-term subduction processes. Of these, long-term subduction processes provided perhaps the best explanation for the observed proximity of uplift/tilting in the east and strong subsidence in the west near Guadeloupe. Models of the response of the overriding plate to differences in the interplate friction coefficient can produce a temporal evolution of coupled uplift and subsidence (Martinod et al., 2016). For example, if a section of plate with reduced coefficient of friction passes beneath a trench, there is a slight uplift of the forearc and arc followed by a subsidence of the volcanic arc as the section passes the over-riding plate Moho. Differences in the coefficient of friction can be caused by

variations in the amount of subducted sediment or inclusion of seafloor features such as seamounts or ridges on the downgoing slab (Martinod et al., 2016). In addition, some studies have proposed that co-seismic deformation associated with megafault activity could contribute to the long-term deformation in the over-riding plate (Taylor et al., 1980).

Irrespective of the exact mechanisms, the evidence from carbonate platforms south of the Kahouanne seamounts clearly indicate subsidence rates on the order of 300 to 400 m/My.If such regional rates also affected the Kahouanne seamounts, then the 50-meter difference cited above could easily be accounted for by considering coupled local (graben-formation) and regional subsidence during a >3 Myr interval from shallow-water carbonate formation to the current outcrop depth of 600 meters. The magnitude of subsidence of the Kahouanne seamounts, ~600 m in 3 Myr, is comparable to rates inferred from other intra-arc basins in oceanic subduction zones. For example, IODP drilling in the Tonga arc of the western Pacific allowed for a detailed assessment of the evolution/subsidence of a small basin along the trend of the volcanic arc (Clift et al., 1994). At site 840 a total subsidence of 500 meters occurred over a period of 2 My.

We suggest that the Kahouanne seamounts were in fact once subaerial volcanoes with their summits well above sea level. The diameters of the craters and dimensions of the cones are similar to other basaltic to andesitic stratovolcanoes in the Lesser Antilles, such as La Soufriere (St Vincent), the Quill (St Eustatius), Mount Liamurga (St Kitts) and Nevis, with present-day altitudes of 1234 m, 601 m, 1156 m and 985 m respectively. Between 5.4 Ma and 3 Ma it would require a subsidence rate of about 400 m/Myr to bring the summit of an approximately 1000 m asl volcano to sea level (even without

accounting for erosion of the edifice over this time period). This is a maximum value as erosion rates of volcanic edifices are high in the Lesser Antilles with values ranging from 200 to 1000 m/My (Rad et al., 2103; Ricci et al., 2015). Subsidence of subaerial edifices could be easily accommodated through a combination of subaerial erosion and subsidence of the order calculated based on the marine samples for the Kahouanne seamounts. Over the longer time interval of 5.4 Ma to present, a combination of regional/local tectonic processes and subaerial erosion can thus plausibly explain the transition of the Kahouanne centers from a subaerial volcanic island(s) to their current depth. Such an evolution would indicate that the seamounts are best described as guyots.

6. Conclusions

Recent multibeam mapping and remotely-operated vehicle (ROV) explorations of the Kahouanne seamounts in the northern Lesser Antilles indicate that the complex was partially subaerial and has subsequently subsided to depths of ~600 meters. The seamounts are thus considered to be guyots. Evidence for previous subaerial exposure and subsidence includes basaltic andesite outcrops with honeycomb weathering features, the terraced morphology of the seamounts, sculpted lava flows, and shallow-water carbonate samples recovered on terraces at 600 meters water depth, themselves also showing coastal erosional features, very likely the result of boring echinoids. This is the first documented occurrence of honeycomb weathering/bioerosional features in the deep sea and their occurrence should be considered a valuable parameter for assessing the subsidence history of oceanic seamounts.

The Kahouanne seamounts formed a polygenetic center of volcanism, erupting varied magma compositions and may have formed an island comparable in scale to some of the smaller islands in the currently active northern Lesser Antilles arc. $^{40}Ar/^{39}Ar$ dating indicates basaltic-andesite volcanism occurred at the Kahouanne seamounts at least until 5.4 Ma ago, but this may have ceased as the arc front migrated east at this latitude, establishing volcanism at its current site on Montserrat. Shallow-water carbonates at the summit of the Kahouanne seamounts (now in deep water) were deposited at about 3 Ma, as inferred from strontium isotope measurements. Subsidence of the seamounts was likely associated with formation of the Kahouanne valley, a half-graben lying between the islands of Montserrat and Guadeloupe, coupled with a regional subsidence component documented at carbonate platforms around the islands of Guadeloupe and Martinique to the south. Interpretation of depth profiles and seismic reflection profiles through the Kahouanne valley suggest that up to 500 meters of subsidence can be attributed to graben formation during the last 3 Myr. The residual 50-100 m, required to explain the current depth of shallow-water carbonates, can either be explained by eustatic sea-level changes, or may alternatively be assigned to regional subsidence affecting large areas of the northern Lesser Antilles. A total subsidence of 600 m during a period of 3 Myr is in accord with observations of subsidence of intra-arc basins in other oceanic subduction zones such as the Tonga Arc in the western Pacific (e.g. Clift et al., 1994).

Acknowledgements

Funding for research cruise NA037 of the *E/V Nautilus* was provided by the Office of Ocean Exploration of the National Oceanic and Atmospheric Administration (NOAA).

We thank the captain and crew of the *Nautilus* for their excellent support during cruise operations. The Montserrat Volcano Observatory (MVO) provided valuable monitoring of the Soufriere Hills volcano while the ship was operating offshore of Montserrat. In addition, the cooperation and assistance of the Seismic Research Unit of the University of West Indies is gratefully acknowledged. MET is grateful to ostracodologists Simone Brandano, Ben Sames, Robin Smith and Tsukagoski Akiri for their comments. We are grateful to John McArthur for permission to reference the LOWESS Sr database. Support for $^{40}Ar/^{39}Ar$ analysis came from grant 1114-1519 to S. Watt from the NERC Argon Isotope Facility. RSJS was supported by a Leverhulme Trust Emeritus Fellowship. The paper benefited from comments and suggestions from Ricardo Ramalho and two other anonymous reviewers.

References

Asgaard, U. & Bromley, R.G., 2008. Echinometrid sea urchins, their trophic styles and corresponding bioerosion. In: Current Developments in Bioerosion, edited by Wisshak, M. & Tapanila, L. Berlin: Springer. pp. 279-303.

Birck, J.L., 1986. Precision K-Rb-Sr isotopic analysis: application to Rb-Sr chronology. Chemical Geology 56, 73-83.

Bouysse, P., Westercamp, D., Andreieff, P., 1990. The Lesser Antilles Island Arc. In: Moore, J.C., Mascle, A., et al. Proc. ODP Sci. Results vol. 110, 29-44.

Buchs, D.M., Williams, R., Sano, S.I., Wright, V.P., 2018. Non-Hawaiian

lithostratigraphy of Louisville seamounts and the formation of high-latitude oceanic islands and guyots. Journal of Volcanology and Geothermal Research, 356, 1-23.

Carey, S.N., 2000. Volcaniclastic sedimentation around island arcs. In: Sigurdsson, H., Houghton, B., McNutt, S.R., Rymer, H., Stix, J. (Eds.), Encyclopedia of Volcanoes. Academic Press, San Diego, p. 627–642.

Carey, S., Schneider, J.L., 2011. Volcaniclastic processes and deposits in the deep-sea. Develop. Sedimentology 63, 457-415.

Carey, S., Bell, K.L.C., Sparks, R.S.J., Stinton, A., Ausubel, J., Phillips, B., Raineault, N., Siu, N., Fandel, C., Graham, O., Ramsingh, H., Blake, R., Auscavitch, S., Demopoulos, A., Rodrigue, K., 2014. Impact of volcanic eruptions on the seafloor around Montserrat, West Indies. In: Bell, K.L.C., M.L. Brennan, and N.A. Raineault, eds. 2014. New frontiers in ocean exploration: The E/V *Nautilus* 2013 Gulf of Mexico and Caribbean field season. Oceanography 27(1), supplement, 52 pp, https://doi.org/10.5670/oceanog.2014.supplement.01.

Cassidy, M., Taylor, R., Palmer, M. R., Cooper, R. J., Stenlake, C., Trofimovs, J., 2012. Tracking the magmatic evolution of island arc volcanism: Insights from a high-precision Pb isotope record of Montserrat, Lesser Antilles. Geochem. Geophys. Geosyst. 13, Q05003, doi:10.1029/2012GC004064.

Cassidy, M., Watt, S. F. L., Talling, P. J., Palmer, M. R., Edmonds, M., Jutzeler, M., Wall-Palmer, D., Manga, M., Coussens, M., Gernon, T. & Taylor, R. N. 2015. Rapid onset of mafic magmatism facilitated by volcanic edifice collapse. Geophysical Research Letters 42(12), 1-7.

Cassidy, M., Edmonds, M., Watt, S.F.L., Palmer, M.R., Gernon, T.M., 2015. Origin of Basalts by Hybridization in Andesite-dominated Arcs. J. Petrol. 56, 325–346. https://doi.org/10.1093/petrology/egv002

Chaytor, J. D., Keller, R. A., Duncan, R. A., Dziak, R. A., 2007, Seamount morphology in the Bowie and Cobb hot spot trails, Gulf of Alaska. Geochem. Geophys. Geosyst. 8, Q09016, doi:10.1029/2007GC001712.

Clague, D., Moore, J., Reynolds, J., 2000. Formation of flat-topped volcanic cones in Hawaii: Bull. Volcanol. 62, 214-233.

Clift, P., and ODP Leg 135 Scientific Party, 1994. Volcanism and sedimentation in a rifting island-arc terrain: an example from Tonga, SW Pacific. Geol. Soc. Lond. Spec. Pub. 81, 29-51.

Coussens, M., Cassidy, M., Watt, S.F.L., Jutzeler, M., Talling, P.J., Barfod, D., Gernon, T.M., Taylor, R., Hatter, S.J., Palmer, M.R., 2017. Long-term changes in explosive and effusive behaviour at andesitic arc volcanoes: Chronostratigraphy of the Centre Hills Volcano, Montserrat. J. Volcanol. Geotherm. Res. 333–334, 15–35. https://doi.org/10.1016/j.jvolgeores.2017.01.003

Coussens, M.F., Wall-Palmer, D., Talling, P.J., Watt, S.F.L, Hatter, S., Cassidy, M., Clare, M., Jutzeler, M., Hatfield, R., McCanta, M., Kataoka, K.S., Endo, D., Palmer, M.R., Stinton, A., Fujinawa, A., Boudon, G., Le Friant, A., Ishizuka, O., Gernon, T., Adachi, T., Aljahdali, M., Breitkreuz, C., Fraas, A.J., Hornbach, M.J., Lebas, E., Lafuerza, S., Maeno, F., Manga, M., Martinez-Colon, M., McManus, J., Morgan, S., Saito, T., Slagle, A., Subramanyam, K.S.V., Tamura, Y., Trofimovs, J., Villemant, B., Wang, F., and the Expedition 340 scientists, 2016. Synthesis: stratigraphy and age

control for IODP Sites U1394, U1395, and U1396 offshore Montserrat in the Lesser Antilles. *In* Le Friant, A., Ishizuka, O., Stroncik, N.A., and the Expedition 340 Scientists, Proceedings of the Integrated Ocean Drilling Program, 340: Tokyo (Integrated Ocean Drilling Program Management International, Inc.). **http://dx.doi.org/ 10.2204/ iodp.proc.340.204.2016**

Druitt, T. H. & Kokelaar, B. P. (eds) 2002. The Eruption of Soufrière Hills Volcano, Montserrat, from 1995 to 1999. Geological Society Memoir no. 21. 645pp

Farrell, J.W., Clemens, S.C., Gromet, P.L., 1995. Improved chronostratigraphic reference curve of late Neogene seawater $^{87}Sr/^{86}Sr$. Geology 23, 403–406.

Feuillet, N., Manighetti, I., Tapponnier, P, Jacques, E., 2002. Arc parallel extension and localization of volcanic complexes in Guadeloupe, Lesser Antills. J. Geophys. Res., 107, 2331.

Feuillet, N., Leclerc, F., Tapponnier, P., Beauducel, F., Boudon, G., Le Friant, A., Deplus, C., Lebrun, J., Necessian, A., Saurel, J.M., Clement, V., 2010. Active faulting induced by slip partitioning in Montserrat and link with volcanic activity: new insights from the 2009 GWADASEIS marine cruise data. Geophys. Res. Lett., 37, 1-6 doi:10.1029/2010GL042554.

Foster, M., Filho, G., Kamenos, N., Riosmena-Rodriguez, R., Stellar, D., 2013. Rhodoliths and rhodolith beds. Smithsonian Contrib. Mar. Sci. 39, 143-155.

Germa, A., Quidelleur, X., Labanieh, S., Chauvel, C., Lahitte, P., 2011. The volcanic evolution of Martinique Island: Insights from K–Ar dating into the Lesser Antilles arc migration since the Oligocene. Jour. Volcanol. Geotherm. Res. 208(3), 122-135.

Gouramanis, C., Wilkins, D., De Deckker, P. , 2010. 6000 years of environmental changes recorded in Blue Lake, South Australia, based on ostracod ecology and valve chemistry. Palaeogeo., Palaeoclim., Palaeoecol., 297, 223–237.

Harford, C. L., Pringle, M. S., Sparks, R. S. J. & Young, S. R. 2002. The volcanic evolution of Montserrat using $^{40}Ar/^{39}Ar$ geochronology. Geological Society, London, Memoirs, 21(1), 93, 95-96, 99-101, 109.

Haq, B., Hardenbol, J., Vail, P., 1988. Mesozoic and Cenozoic chronostratigraphy and cycles of sea-level change. SEPM Special Publication, No. 42, 71-108.

Hatter, S.J., Palmer, M.R., Gernon, T.M., Taylor, R.N., Cole, P.D., Barfod, D.N., Coussens, M., 2018. The Evolution of the Silver Hills Volcanic Center, and Revised 40 Ar/ 39 Ar Geochronology of Montserrat, Lesser Antilles, With Implications for Island Arc Volcanism. Geochemistry, Geophys. Geosystems 19, 427–452. https://doi.org/10.1002/2017GC007053

Heuser, A., Eisenhauer, A., Gussone, N., Bock, B., Hansen, B.T., Nägler, T.F., 2002. Measurement of calcium isotopes (δ44Ca) using a multicollector TIMS technique. International Journal of Mass Spectrometry 220, 385-397.

Hess, H., 1946. Drowned ancient islands of the Pacific Basin. Amer. Jour. Sci. 244, 772-791.

Howarth, R.J., McArthur, J.M., 1997. Statistics for Strontium Isotope Stratigraphy: A robust LOWESS fit to the marine Sr-isotope curve for 0 to 206 Ma, with look-up table for derivation of numeric age. Journal of Geology, 105, 441–456.

Ingersoll, R., 2001. Tectonics of sedimentary basins with revised nomenclature (Chapter 1). Tectonics of Sedimentary Basins, Recent Advances (C. Busby and A. Azor, eds.). Wiley, https://doi.org/10.1002/9781444347166.ch1.

Kameo, K., Shearer, M.C., Droxler, A.W., Mita, I., Watanabe, R., Sato, T., 2004. Glacial–interglacial surface water variations in the Caribbean Sea during the last 300 ky based on calcareous nannofossil analysis. Palaeogeography, Palaeoclimatology, Palaeoecology 212, 65– 76.

Karig, D., 1971. Structural history of the Mariana island arc system. Geol. Soc. Amer. Bull. 82(2), 323-344.

Kázmér, M., Leman, M.S., Mohamed, K.R., Ali, C.A. & Taboroši, D., 2015. Features of intertidal bioerosion and bioconstruction on limestone coasts of Langkawi Islands, Malaysia. Sains Malaysiana 44, 921–929.

Labanieh, S., Chauvel, C., Germa, A., Quidelleur, X., Lewin, E., 2010. Isotopic hyperbolas constrain sources and processes under the Lesser Antilles arc. Earth and Planetary Science Letters 298, 35-46.

Lebas, E., Le Friant, A., Boudon, G., Watt, S. F. L., Talling, P. J., Feuillet, N., Deplus, C., Berndt, C., Vardy, M. E., 2011. Multiple widespread landslides during the long- term evolution of a volcanic island: Insights from high- resolution seismic data, Montserrat, Lesser Antilles. Geochem. Geophys. Geosyst. 12, Q05006, doi:10.1029/2010GC003451.

Leclerc, F. and Feuillet, N., 2019. Quaternary coral reef complexes as powerful markers of long-term subsidence related to deep processes at subduction zones: Insights from Les Saintes (Guadeloupe, French West Indies). Geosphere, 15, 1-25.

Leclerc, F., Feuillet, N., Cabioch, G., Deplus, D., Lebrun, J., BATHSAINTES cruise scientific party, Bazin, S., Beauducel, G., Boudon, G., LeFriant, A., De Min, L., Melezan, D., 2014. The Holocene drowned reef of Les Saintes plateau as witness of a long-term tectonic subsidence along the Lesser Antilles volcanic arc in Guadeloupe. Mar. Geol., 355, 115-135.

Leclerc, F., Feuillet, N., Perret, M., Cabioch, G., Bazin, S., Lebrun, J., Saurel, J.M., 2015. The reef platform o Martinique: Interplay between eustasy, tectonic subsidence and volcanism since late Pleistocene. Mar. Geol. 369, 34-51.

Le Friant, A., Harford, C. L., Deplus, C., Boudon, G., Sparks, R. S. J., Herd, R. A., Komorowski, J.- C. , 2004. Geomorphological evolution of Montserrat (West Indies): Importance of flank collapse and erosional processes. J. Geol. Soc. 161, 147–160, doi:10.1144/0016-764903-017.

Le Friant, A., Ishizuka, O., Boudon, G., Palmer, M.R., Talling, P.J., Villemant, B., Adachi, T., Aljahdali, M., Breitkreuz, C., Brunet, M., Caron, B., Coussens, M., Deplus, C., Endo, D., Feuillet, N., Fraas, A.J., Fujinawa, A., Hart, M.B., Hatfield, R.B., Hornbach, M., Jutzeler, M., Kataoka, K.S., Komorowski, J.-C., Lebas, E., Lafuerza, S., Maeno, F., Manga, M., Martínez-Colon, M., McCanta, M., Morgan, S., Saito, T., Slagle, A., Sparks, S., Stinton, A., Stroncik, N., Subramanyam, K.S.V., Tamura, Y., Trofimovs, J., Voight, B., Wall-Palmer, D., Wang, F., Watt, S.F.L., 2015. Submarine record of volcanic island construction and collapse in the Lesser Antilles arc: first scientific drilling of submarine volcanic island landslides by IODP Expedition 340. Geochem., Geophys., Geosy. 16(2), 420–442. **http://dx.doi.org/ 10.1002/ 2014GC005652**

Lewis, J., Coath, C., Pike, A., 2014. An improved protocol for 87Sr/86Sr by laser ablation multi-collector inductively coupled plasma mass spectrometry using oxide reduction and a customised plasma interface. Chemical Geology 390, 173-181.

Marack, E., 1999. The relationship between water motion and living rhodolith beds in the southwestern Gulf of California, Mexico. Palaios 14, 159-171.

Martin- Kaye, P. H. A., 1969. A summary of the geology of the Lesser Antilles, Overseas Geol. Miner. Resour. 10(2), 172–206.

Martinod, J., Regard, V., Letourmy, Y., Henry, H., Hassani, R., Baratchart, S., Carretier, S., 2016, How do subduction processes contribute to forearc Andean uplift?: Insights from numerical models: Journal of Geodynamics, 96, 6–18. https:// doi .org /10 .1016 /j .jog .2015 .04 .001

McArthur, J.M., Rio, D., Massari, F., Castradori, D., Bailey, T.R., Thirlwall, M. & Houghton, S., 2006. A revised Pliocene record for marine-87Sr/86Sr used to date an interglacial event recorded in the Cockburn Island Formation, Antarctic Peninsula. Palaeogeography, Palaeoclimatology, Palaeoecology 242, 126–136.

Mustoe, G., 1982. The origin of honeycomb weathering. Geol. Soc. Amer. Bull. 93, 108-115.

Paduan, J., Clague, D., Davis, A., 2009. Evidence that three seamounts off southern California were ancient islands. Mar. Geol. 265, 146-156.

Pérez, L., Lorenschat, J., Bugja, R., Brenner, M., Scharf, B., Schwalb, A., 2010. Distribution, diversity and ecology of modern freshwater ostracodes (Crustacea), and

hydrochemical characteristics of Lago Petén Itzá, Guatemala. J. Limnol., 69, 146-159, DOI: 10.3274/JL10-69-1-14.

Rad, S., Rivé, K., Vittecoq, B., Cerdan, O., Allègre, C.J., 2013. Chemical weathering and erosion rates in the Lesser Antilles: An overview in Guadeloupe, Martinique and Dominica. Journal of South American Earth Sciences, 45, 331–344. https:// doi .org /10 .1016 /j .jsames .2013 .03 .004.

Rebelo, A.C., Rasser, M., Kroh, A., Johnson, M.E., Melo, C., Ramalho, R.S., Uchman, A., Zanon, V., Silva. L., Neto, A., Berning, B., Cachão, M., Ávila, S., 2015. Rocking around a volcanic island shelf: neogene rhodolith beds from Malbusca, Santa Maria Island (Azores, NE Atlantic). Facies, 62:22, pp 31.

Ricci, J., Lahitte, P., Quidelleur, X., 2015. Construction and destruction rates of volcanoes within tropical environment: Examples from the Basse-Terre Island (Guadeloupe, Lesser Antilles): Geomorphology, 228, 597–607. https:// doi .org /10 .1016 /j .geomorph .2014 .10 .002.

Ricchi, A., Quartau, R., Ramalho, R.S., Romagnoli, C., Casalbore, D., da Cruz, J.V., Fradique, C. ,Vinhas, A., 2018. Marine terrace development on reefless volcanic islands: New insights from high-resolution marine geophysical data offshore Santa Maria Island (Azores Archipelago). Marine Geology 406, 42–56.

Rodriguez-Navarro, C., Doehne, E., Sebastian, E., 1999. Origins of honeycomb weathering: the role of salts and wind. Geology 111, 1250-1255.

Rutherford, M., Devine, J., 2003. Magmatic conditions and magma ascent as indicated by hornblende phase equilibria and reactions in the 1995-2001 Soufriere Hills magma. Jour. Petrol. 44, 1433-1454.

Samper, A., Quidelleur, X., Lahitte, P., and Mollex, D., 2007, Timing of effusive volcanism and collapse events within an oceanic arc island: Basse-Terre, Guadeloupe archipelago (Lesser Antilles Arc): Earth Planet. Sci.Lett. 258, 175–191.

Schwartz, D., Soule, A., Wanless, D., Jones, M., 2018. Identification of erosional terraces on seamounts: implications for interisland connectivity and subsidence in the Galapagos Archipelago. Front. Earth. Sci. 6 (88), 1-17.

Swart, P. 2015. The geochemistry of carbonate diagenesis: The past, present and future. Sedimentology, 62, 1233–1304.

Taylor, F.W., Isacks, B.L., Jouannic, C., Bloom, A.L., Dubois, J., 1980, Coseismic and Quaternary vertical tectonic movements, Santo and Malekula Islands, New Hebrides Island Arc: Journal of Geophysical Research. Solid Earth, 85, no. B10, 5367–5381. https:// doi .org /10 .1029 /JB085iB10p05367.

Thien, B.M.J., Kosakowski, G., Kulik, D.A., 2015. Differential alteration of basaltic lava flows and hyaloclastites in Icelandic hydrothermal systems. Geothermal Energy 3, 11.

Trenhaile, A.S., 1987, The geomorphology of rocky coasts: Oxford, Clarendon Press, 384 p.

Trofimovs, J., Fisher, J.K. Macdonald, H.A, Talling, P.J., Sparks, R.S.J., Hart, M.B., Smart, C., Boudon, G., Deplus, C., Komorowski, J-C., Le Friant, A., Moreton, S.G., ,Leng, M.J. 2010. Evidence for carbonate platform failure during rapid sea-level rise; ca 14,000 year old bioclastic flow deposits in the Lesser Antilles. Sedimentology 57, 735-739.

Tucker, M.E. & Wright, V.P., 1990. Carbonate Sedimentology. Blackwell Science. Oxford, 496 p..

Wadge, G., Voight, B., Sparks, R.S.J., Cole, P., and Loughlin, S.C. 2014. An Overview of the Eruption of Soufriere Hills Volcano from 2000-2010. In "*The Eruption of the Soufriere Hills Volcano, Montserrat from 2000-2010*" edited by Wadge, G., Robertson, R.A.E. and Voight, B. Geological Society Memoir 39, 1-40.

Watt, S.F.L., Talling, P.J., Vardy, M.E., Masson, D.G., Henstock, T.J., Hühnerbach, V., Minshull, T.A., Urlaub, M., Lebas, E., Le Friant, A., Berndt, C., Crutchley, G.J., Karstens, J., 2012. Widespread and progressive seafloor-sediment failure following volcanic debris avalanche emplacement: landslide dynamics and timing offshore Montserrat, Lesser Antilles. Mar. Geol. 323–325, 69–94. **doi:10.1016/ j.margeo.2012.08.002**

Wessel, P., 1997. Sizes and ages of seamounts using remote sensing: implications for intraplate volcanism. Science 277, 802–805.

Yamaji, A., 1990. Rapid intra-arc rifting in Miocene northeast Japan. Tectonics 9(3), 365-378.

Zellmer, G. F., Hawkesworth, C. J., Sparks, R. S. J., Thomas, L. E., Harford, C. L., Brewer, T. S. & Loughlin, S.C. 2003. Geochemical evolution of the Soufriere Hills volcano, Montserrat, Lesser Antilles volcanic arc. *Journal of Petrology*, **44**(8), 1349-1352, 1357, 1370-1371.

Zwalinska, K., Dabski, M., 2010. Cavernous weathering forms in SE Iceland: a case study on weathering of basalts in a cold temperature maritime climate: Miscellanea Geographica 16, 11-16.

Figure Captions

Figure 1 Map showing the location of the Kahouanne Seamounts southeast of the island of Montserrat. Principal volcanic centers on Montserrat are marked by red triangles. Faults are indicated based on Feuillet et al. (2010) and on interpretation of seismic reflection data in Watt et al. (2012). The seamounts lie on the eastern side of a graben, the Kahouanne valley, bordered on southwest by the major Bouillante-Montserrat fault system. The inset map shows the location of the study region within the Lesser Antilles. Locations of seismic reflection lines and bathymetric profiles in shown in Figs. 2 and 14 are indicated by the blue and green lines that cross the Kahouanne valley.

Figure 2. Interpreted seismic reflection profiles (upper two) cf. Watt et al., 2012) across the Kahouanne Valley and the western margins of the Kahouanne seamounts (profile locations in Fig. 1). Deposits 2 and 8 are major mass-wasting deposits from Montserrat, and the base Centre Hills horizon marks the mapped horizon beneath the offshore Centre Hills debris fan (Watt et al., 2012; ~950 ka). The uppermost Kahouanne seamount horizon has been interpreted across the basin, with selected reflections in the seamounts also highlighted to emphasize structural complexities in these polygenetic volcanoes. Lower profile (gwa-039) modified from Feuillet et al. (2010).

Figure 3. a) multibeam bathymetric map of the Kahaoanne seamounts southeast of Montserrat (box indicates the potential debris field from an avalanche on the northwest

side of the central seamount). Color coded by depth in meters. b) backscatter image of the same area. Light shades of gray indicate high reflectivity seafloor and dark shades correspond to softer, likely sediment-covered surfaces. Possible faults are highlighted by red dashed lines and are oriented in the same general NE to SE trend as other faults in the Montserrat-Havre and Bouillante-Montserrat fault systems (see figure 1).

Figure 4. a) Perspective multibeam bathymetric map of the Kahaoanne seamounts with a 2:1 vertical exaggeration showing the relatively flat tops of the central and northern centers A and B. A smaller, deeper seamount (C) with a well-defined circular crater lies to the southeast of seamount B. Numbers on horizontal and vertical scales are in meters. Locations of ROV images presented in figures 5-7 are shown by red circles, b) plan view bathymetric map of the central seamount B and southern crater C. Trackline for ROV dive H1311 is shown as black line (dashed section of dive track indicates area where the ROV was not in visual range of the seafloor). The roughly circular crater in seamount B contain several small domes and a prominent spire on the southeast rim. ROV sample localities are shown by black circles.

Figure 5. ROV images in the southern Kahouanne seamount C showing a) poorly-sorted volcaniclastic deposit with rounded clasts encrusted with manganese exposed in the crater wall (red bar is 10 cm in length), and b) sculpted and fractured lava flow outcrop with manganese coating (small fish for scale). Location of images a and b shown in figure 4a.

Figure 6. ROV images from the central Kahouanne seamount B showing a) honeycomb texture on an andesite boulder (width of boulder is about 2 meters across). The boulders occur on the southern side of the main terrace of the seamount at a depth of about 600 m , b) sculpted andesite lava (height of outcrop is about 1.5 meters) with a remnant pillow structure near the center of the outcrop, c) honeycomb texture on andesite boulder showing linear alignment of pock-marks (width of boulder is about 2 meters), and d) honeycomb texture on andesite lava outcropping on the side of a spire in the central Kahouanne seamount (width of field of view is about 3 meters). Locations of images a b,c, and d are shown in figure 4a.

Figure 7. a) Sculpted lava outcrop in the crater of the central seamount B with manganese coating. Maximum width of outcrop is about 1.5 meters., b) Rectangular fracture pattern in andesite lava outcrop near small domes in the central seamount B. Slab-like morphology of the flow suggests possible emplacement as a sheet flow. Vertical whip coral growing on flow surface is about 0.5 meters long. c) Open bivalve shells mixed with branching coral debris on the crater floor of the central seamount B. Shells and coral fragments are coated with a thin veneer of unconsolidated hemipelagic sediment. Red laser dots are 10 cm apart. Locations of images a b, and c, are shown in figure 4a.

Figure 8. a) Volcaniclastic sandstone NA037-50 from Kahouanne seamount C (width of image is about 6 cm), b) Photomicrograph of sample NA037-50 showing vesicular oxidized pyroclastics and crystals (plain light). Reddish, oxidized features of the sample suggest eruption under subaerial conditions. Details of circled area is shown in image c.

Photomicrograph of ostracod shells in between grains of the volcaniclastic sandstone (crossed polarizer). Scale bar is 50 microns. d) Photomicrograph of poorly vesicular andesite lava NA037-55 from the crater of Kahouanne seamount B showing hornblende with reaction rims and plagioclase phenocyrsts (crossed polarizer). Scale bar is 1000 microns. Locations of images a b,c, and d are shown in figure 4a.

Figure 9. $^{40}Ar/^{39}Ar$ plateau age determinations for plagioclase crystals from samples NA037-052 (top) and NA037-055 (bottom) from the Kahouanne seamount B. A photomicrograph of NA037-055 is shown in figure 8d. Both samples have roughly similar ages of slightly older than 5 Ma. The locations of samples are shown in figure 4b.

Figure 10. Images of carbonate sample NA037-053 from the 600 m deep terrace on Kahouanne seamount B. a) cut section showing prominent rhodoliths, 1-2 cm in diameter with bioclastic sediment between containing benthic foraminifer and other shallow-water bioclasts (scale in cms). In addition there is a much later internal sediment (pale brown-tope in color), containing planktic forams. An Fe-Mn crust coats a very irregular upper surface. Note the empty holes, probably recent sponge and polychaete borings. b) shallow-water foraminiferas *Amphistegina* and *Peneroplis* in NA037-53 (crossed polarizer), c) Rhodolith bioclastic limestone in plain light, d) Foraminifera (*Amphistegina* central, *Globorotalid* left) with syntaxial fibrous calcite (crossed polarizer). The location of the sample is shown in figure 4b.

Figure 11. Images of carbonate sample NA037-057 from the Kahouanne seamount B. a) deep-water coral in hard limestone full of planktic foraminifera. Note that the coral skeleton was bored, before being buried in pelagic sediment, and then later the lithified limestone was itself bored by sponges. b) planktic foraminifera in fine grain matrix (crossed polarizer), c) deep water coral fragments showing evidence of boring and filling with sediment (crossed polarizer), d) sponge borings into pelagic limestone and coral fragments; spicules present in most recent bore at top. Note central boring in coral is lined with Fe-Mn coating whereas other borings are not. The location of the sample is shown in figure 4b.

Fig. 12. Stable isotope analyses of carbonate samples from Kahouanne seamounts B and C. The 4 samples on the right are the pelagic (deep water) limestones (NA037-047, 886 m depth (black circles) and NA037-057, 666 m depth (blue circles); the 4 samples on the left are the shallow-water limestone (NA037-053, 616 m (red circles)), the sample with +2 C and +1.39 Ox (orange circle) being a carb-phosphate crust on top surface of sample 053. Locations of samples are shown in figure 4b.

Figure 13. a) bathymetry of the Kahouanne seamounts color-coded in meters. Solid black lines indicate bathymetric profile over inferred wave-cut terraces shown in figure 13, b) slope map of the same area color coded by angle in degrees. Inferred wave cut terraces on the seamounts are characterized by slopes of <2 degrees.

Figure 14. Bathymetric profiles across Kahouanne seamounts B (A-A', B-B') and

C (C-C', D-D'). Profile locations are shown in figure 13. Both seamounts exhibit flat tops lying at about 600 meters depth for the central and 650 meters depth for the northern seamounts. Neither flat areas on the central and northern seamounts appears to be tilted in any particular direction.

Figure. 15 Bathymetric profile across the Kahouanne Valley and the central Kahouanne Seamount B (location in Fig. 1). A background increase in depth from NE to SW is offset by the Kahouanne valley graben. Sediment accumulation above the uppermost Kahouanne seamount horizon is indicated (interpolated from seismic reflection data). In addition to the current depth of the graben, this has been used to infer subsidence rates of the seamounts.

Table 1. Kahouanne Seamount Samples

Sample Number	Dive No.	Date (y/m/d)	Time (GMT)	Latitude			Longitude			Depth (m)	Description
NA037-047	H1311	13/10/26	18:25	16	35.9986	N	061	56.0154	W	885	Brown, manganese coated limestone
NA037-049	H1311	13/10/26	21:00	16	36.2806	N	061	56.3354	W	801	Greenish-grey plag- and amphibole-phyric andesite, slightly altered.
NA037-050	H1311	13/10/26	21:29	16	36.2795	N	061	56.3441	W	797	Reddish-brown volcaniclastic sandstone w. some lithic clasts. (Small clasts are highly oxidized).
NA037-051	H1311	13/10/26	22:09	16	36.3397	N	061	56.3866	W	759	Greenish-grey plag-bearing andesite w. concoidal weathering and manganese crust.
NA037-052	H1311	13/10/27	00:35	16	37.1241	N	061	57.0617	W	616	Greenish-grey plag-bearing andesite w. concoidal weathering and manganese crust.
NA037-053	H1311	13/10/27	00:16	16	37.1061	N	061	57.0464	W	616	Brownish white highly-indurated carbonate.
NA037-055	H1311	13/10/27	04:57	16	37.3160	N	061	57.4462	W	652	Hornblende andesite w. complete manganese coating and bio-encrustation. Concoidally weathered surface.
NA037-057	H1311	13/10/27	08:51	16	37.5764	N	061	57.5010	W	666	Very porous carbonate hardpan w. manganese crust.
NA037-058	H1311	13/10/27	10:15	16	37.6244	N	061	57.4620	W	652	Buff grey hornblende-phyric andesite. Concoidally weathering.

Table 2. Carbon and oxygen stable isotope analyses of Kahouanne carbonate samples

Sample Name	$\delta^{18}O$	$\delta^{13}C$
NA037-047a	+3.61	+1.46
NA037-047b	+3.82	+1.85
NA037-057a	+3.33	+2.21
NA037-057b	+3.60	+2.41
NA037-053a	+2.25	+2.32
NA037-053b	+1.99	+2.12
NA037-053c	+1.43	+2.52
NA037-053d	+2.00	+1.39

Table 3. $^{40}Ar/^{39}Ar$ Dating Results for Kahouanne Seamount Samples

					Plateau calculation results											
Sample	RUN	material	J	±J	Ca/K	±2σ	Age (Ma)	±2σ w/o J	±2σ w/J	MSWD	p	Steps	N	N-total	%gas
NA03 7-052	1	plagioclase	0.00054 59	0.00000 54	110.1	0.2	**5.37**	0.53	**0.56**	1.2	0.24	C-P	14	16	99
NA03 7-055	1	plagioclase	0.00054 82	0.00000 57	153.2	1.0	5.50	0.27	0.27	1.0	0.44	H-M	6	6	73
NA03 7-055	2	plagioclase	0.00054 82	0.00000 57	172.3	2.2	5.12	0.33	0.35	1.3	0.18	J-O	6	6	55
NA03 7-055	composite	plagioclase	0.00054 82	0.00000 57	161.7	1.8	**5.38**	0.18	**0.24**	1.4	0.18	H-O	22	22	100

			Inverse isochron calculation results								Integrated age calculation results					
Sample	RUN	material	Age (Ma)	±2σ w/o J	$^{40}Ar/^{36}Ar_{(i)}$	±2σ	MSWD	p	n	Ca/K	±2σ	40Ar*/39ArK	±2σ	Age (Ma)	±2σ
NA03 7-052	1	plagioclase	5.2	0.7	301.8	6.2	1.2	0.26	14	110	5	5.48	0.28	5.4	0.5
NA03 7-055	1	plagioclase	5.6	0.3	298.2	4.1	1.1	0.35	6	156	2	5.28	0.26	5.2	1.1
NA03 7-055	2	plagioclase	5.1	0.6	298.9	2.1	1.5	0.19	6	179	0	5.00	0.28	4.9	1.7
NA03 7-055	composite	plagioclase	5.4	0.3	298.4	5.5	1.5	0.12	12	162	3	5.44	0.11	5.4	0.2

Nucleogenic production ratios:	Isotopic constants and decay rates:

	2.64		
$(^{36}Ar/^{37}Ar)_{Ca}$	$\times 10^{-4}$	$\lambda(^{40}K_{e})$/yr	$5.757 \pm 0.016 \times 10^{-11}$
$(^{39}Ar/^{37}Ar)_{Ca}$	6.5×10^{-4}	$\lambda(^{40}K_{\beta-})$/yr	$4.955 \pm 0.013 \times 10^{-10}$
$(^{38}Ar/^{37}Ar)_{Ca}$	$0.196 \pm 0.00816 \times 10{-}4$	$\lambda(^{37}Ar)$/d	$1.983 \pm 0.0045 \times 10^{-2}$
$(^{40}Ar/^{39}Ar)_{K}$	8.5×10^{-3}	$\lambda(^{39}Ar)$/d	$7.068 \pm 0.0788 \times 10^{-6}$
$(^{38}Ar/^{39}Ar)_{K}$	$1.22 \pm 0.0027 \times 10^{-2}$	$\lambda(^{36}Cl)$/d	$6.308 \pm 0 \times 10^{-9}$
$(^{36}Ar/^{38}Ar)_{Cl}$	$2.629 \pm 0.011 \times 10^{2}$	$(^{40}Ar/^{36}Ar)_{Atm}$	298.56 ± 0.31
$^{37}Ar/^{39}Ar$ to Ca/K	1.96	$(^{40}Ar/^{38}Ar)_{Atm}$	1583. 5 ± 2.5
$^{38}Ar/^{39}Ar$ to Cl/K	2.9	$^{40}K/K_{Total}$	0.01167 ± 0.00002

J : neutron flux parameter
p : probability that residuals can be explained by measurement errors alone
MSWD : mean square weighted deviation (reduced chi-squared statistic)
N : number of steps used in age calculation
N-total : total number of degassing steps attempted
%gas : fraction of 39Ar released in all plateau steps

Table 4. Strontium Isotope Analyses of Kahouanne Seamount Carbonate Samples

Sample Name	Lab Num.	$^{87}Sr/^{86}Sr$	2SE
NA037-047	047A	0.709156	0.000006
NA037-047	047B	0.709154	0.000006
NA037-057	TL33-01	0.709164	0.000005
NA037-057	TL33-02	0.709161	0.000005
NA037-057	TL33-03	0.709168	0.000005
NA037-053	TL33-04	0.70906	0.000005
NA037-053	TL33-05	0.709062	0.000005
NA037-053	TL33-06	0.70909	0.000006
NA037-053	TL33-07	0.709058	0.000006
NA037-053	TL33-08	0.709066	0.000006
NA037-053	TL33-09	0.709061	0.000006

Highlights

1. Honeycomb weathered outcrops discovered at 600 meters water depth in the Caribbean Sea

2. Kahouanne seamount volcanism dated at 5.4 Ma in the Lesser Antilles

3. Shallow water carbonates recovered from 600 meters water depth dated at 2.2 Ma based on strontium isotopes

4. Kahouanne seamounts were likely subaerial volcanoes that have subsided to 600 meters water depth

Figure 1

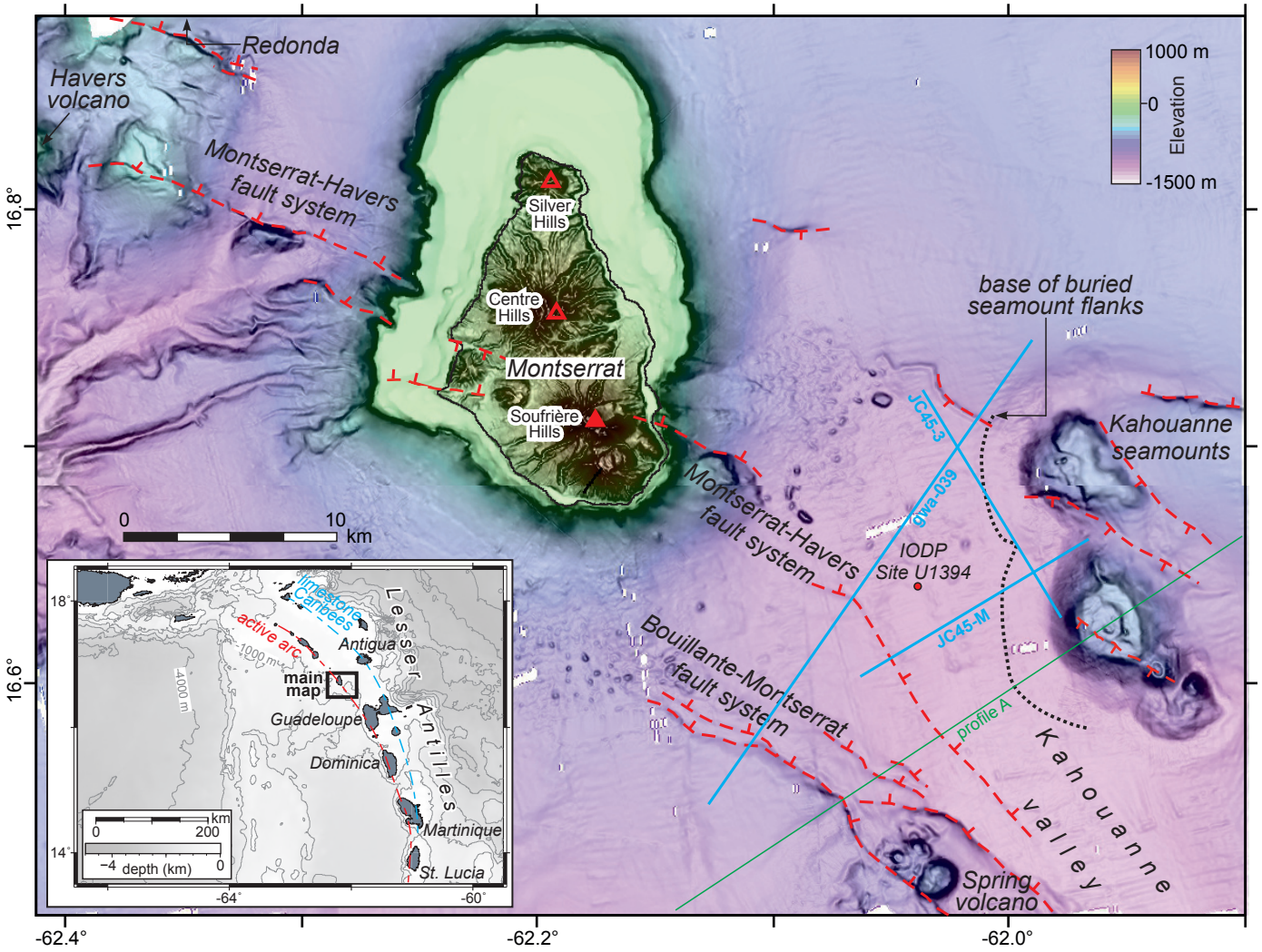
Redonda
Havers volcano
Montserrat-Havers fault system
Silver Hills
Centre Hills
Montserrat
Soufrière Hills
1000 m
0
-1500 m
Elevation
base of buried seamount flanks
Kahouanne seamounts
JC45-3
gwa-039
IODP Site U1394
JC45-M
Montserrat-Havers fault system
Bouillante-Montserrat fault system
profile A
Kahouanne valley
Spring volcano
0
10
km
16.8°
16.6°
-62.4°
-62.2°
-62.0°
18°
14°
-64°
-60°
active arc
Limestone Caribees
Lesser Antilles
Antigua
main map
Guadeloupe
Dominica
Martinique
St. Lucia
1000 m
4000 m
km
0
200
−4
depth (km)
0

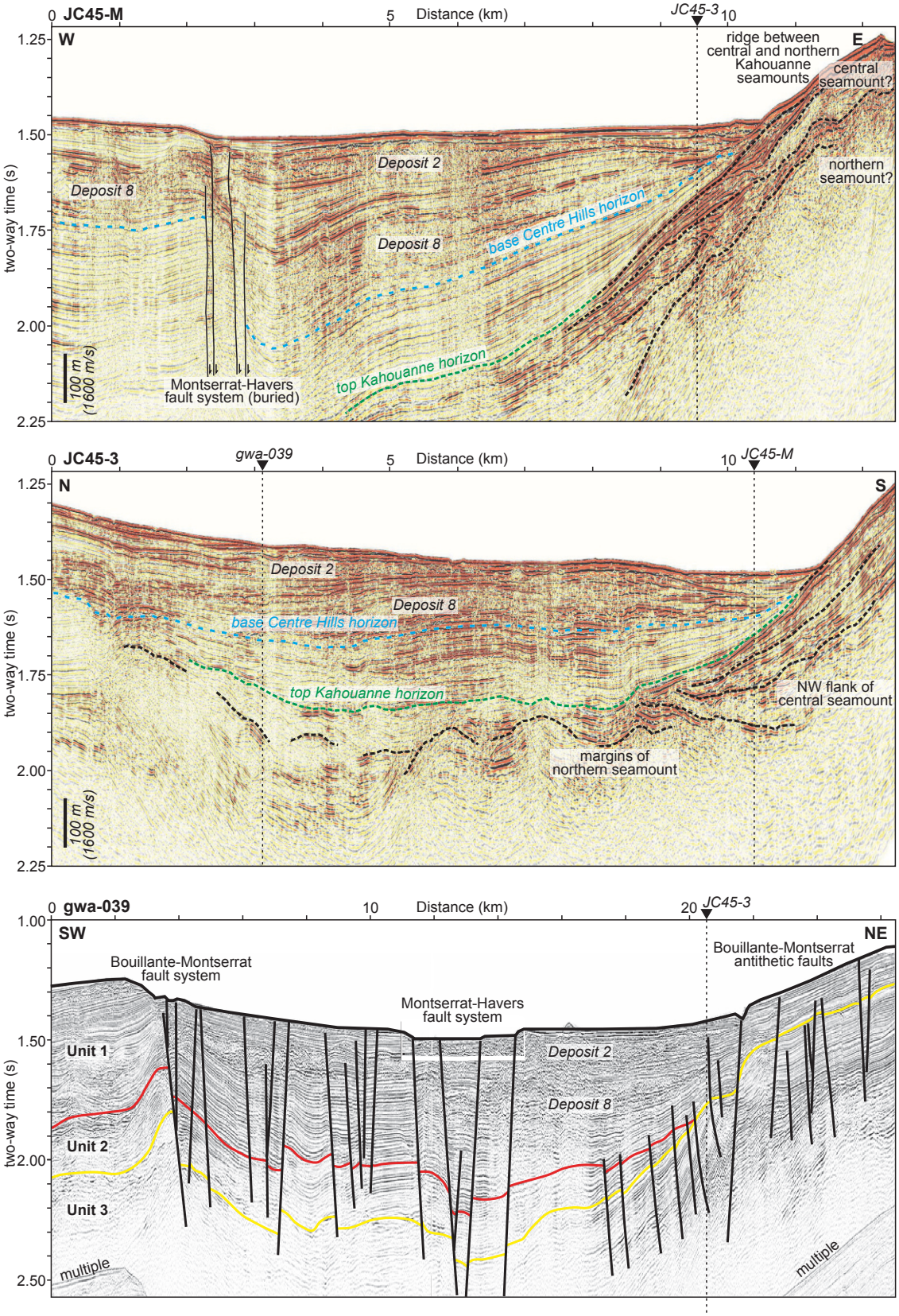
0 JC45-M
5 Distance (km)
JC45-3
10
W
E
ridge between central and northern Kahouanne seamounts
central seamount?
northern seamount?
Deposit 2
Deposit 8
Deposit 8
base Centre Hills horizon
top Kahouanne horizon
Montserrat-Havers fault system (buried)
100 m (1600 m/s)
two-way time (s)
1.25
1.50
1.75
2.00
2.25
0 JC45-3
gwa-039
5 Distance (km)
10 JC45-M
N
S
Deposit 2
Deposit 8
base Centre Hills horizon
top Kahouanne horizon
NW flank of central seamount
margins of northern seamount
100 m (1600 m/s)
two-way time (s)
1.25
1.50
1.75
2.00
2.25
0 gwa-039
10 Distance (km)
20 JC45-3
SW
NE
Bouillante-Montserrat fault system
Montserrat-Havers fault system
Bouillante-Montserrat antithetic faults
Unit 1
Unit 2
Unit 3
Deposit 2
Deposit 8
multiple
multiple
two-way time (s)
1.00
1.50
2.00
2.50

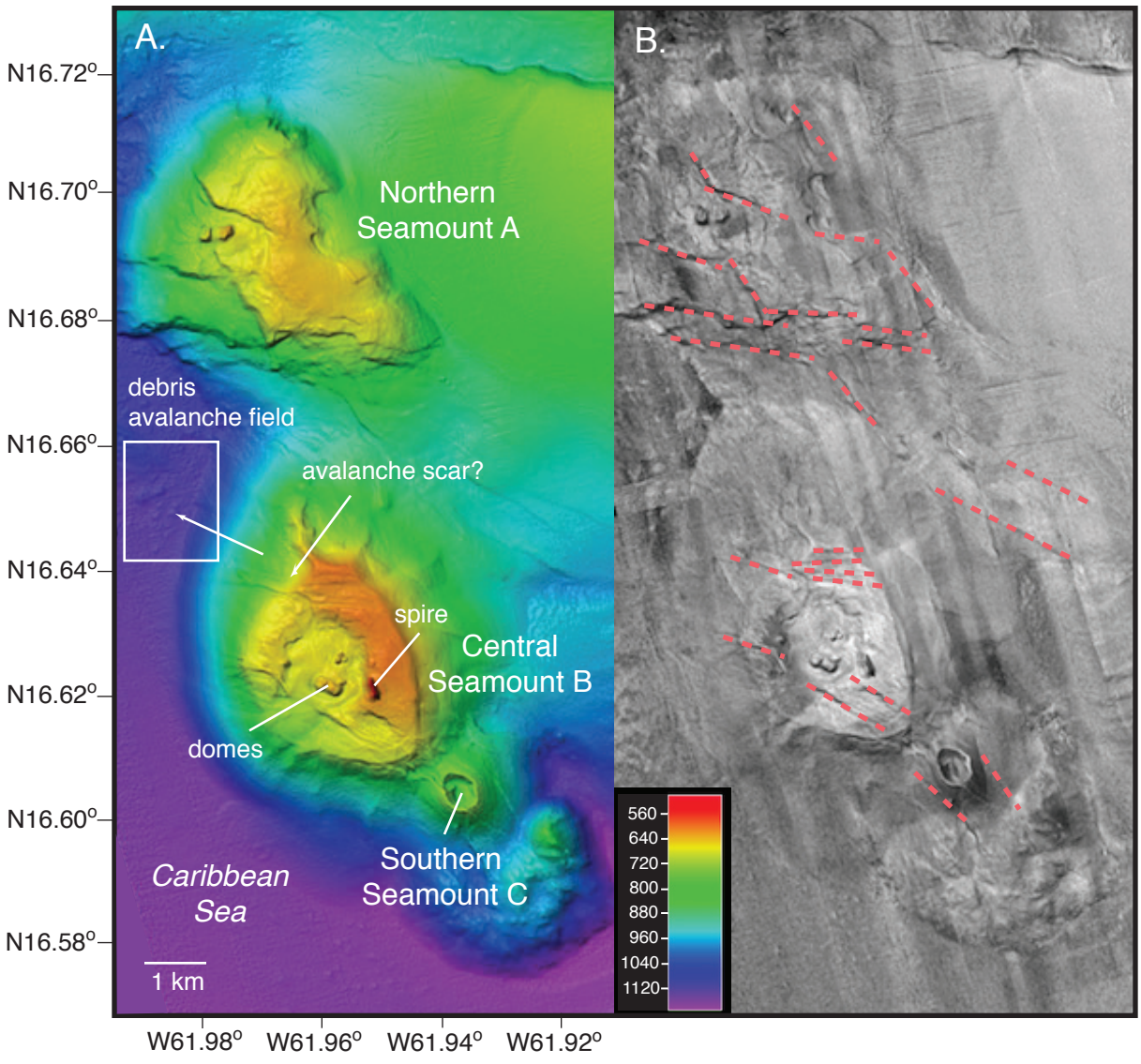
A.
B.
N16.72°
N16.70°
N16.68°
N16.66°
N16.64°
N16.62°
N16.60°
N16.58°
W61.98°
W61.96°
W61.94°
W61.92°
Northern
Seamount A
debris
avalanche field
avalanche scar?
spire
Central
Seamount B
domes
Southern
Seamount C
Caribbean
Sea
1 km
560
640
720
800
880
960
1040
1120

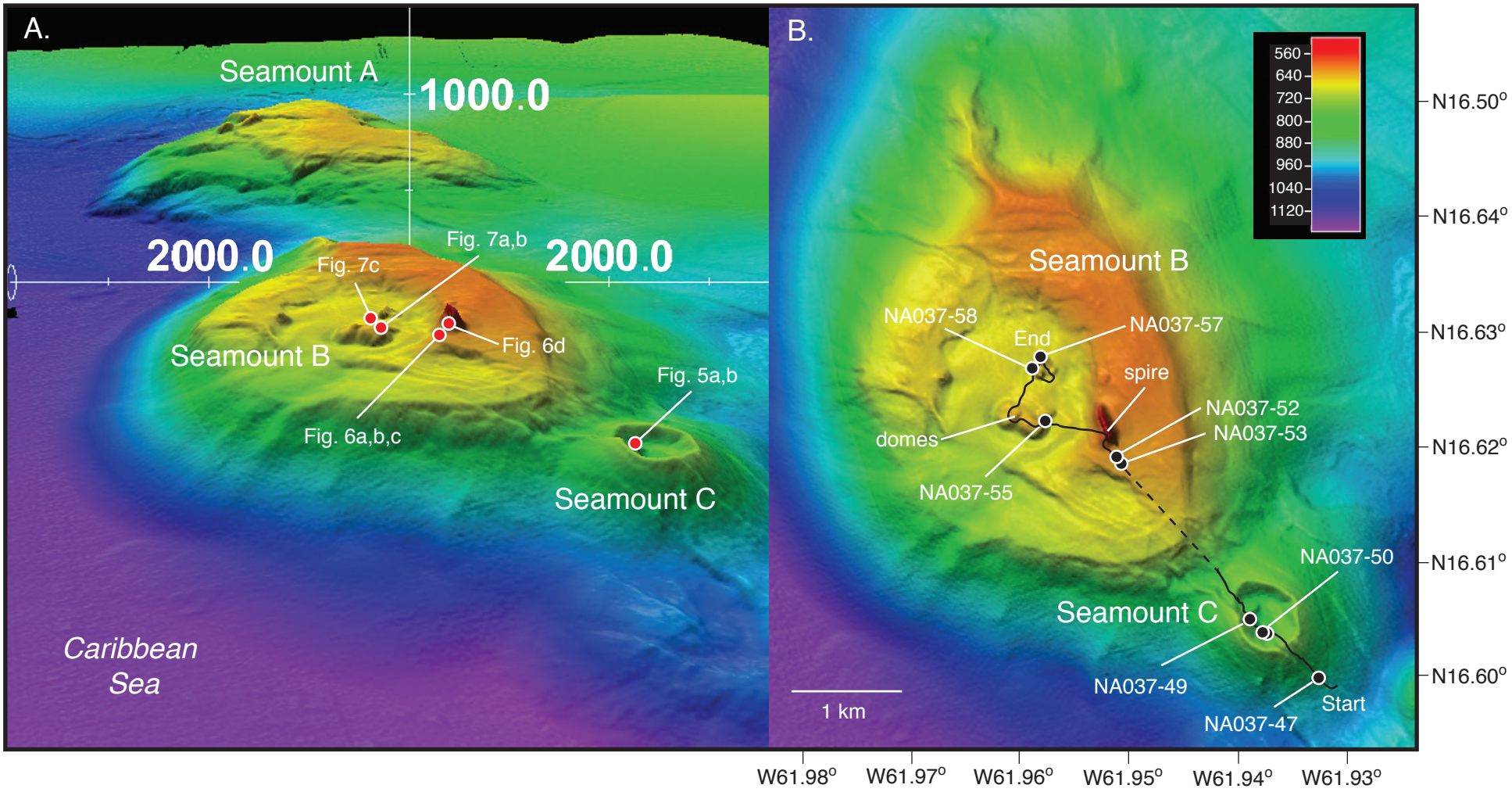
A.
Seamount A
1000.0
2000.0
2000.0
Fig. 7c
Fig. 7a,b
Fig. 6d
Seamount B
Fig. 5a,b
Fig. 6a,b,c
Seamount C
Caribbean
Sea
B.
560
640
720
800
880
960
1040
1120
Seamount B
NA037-58
End
NA037-57
spire
NA037-52
NA037-53
domes
NA037-55
NA037-50
Seamount C
NA037-49
Start
NA037-47
1 km
N16.50°
N16.64°
N16.63°
N16.62°
N16.61°
N16.60°
W61.98°
W61.97°
W61.96°
W61.95°
W61.94°
W61.93°

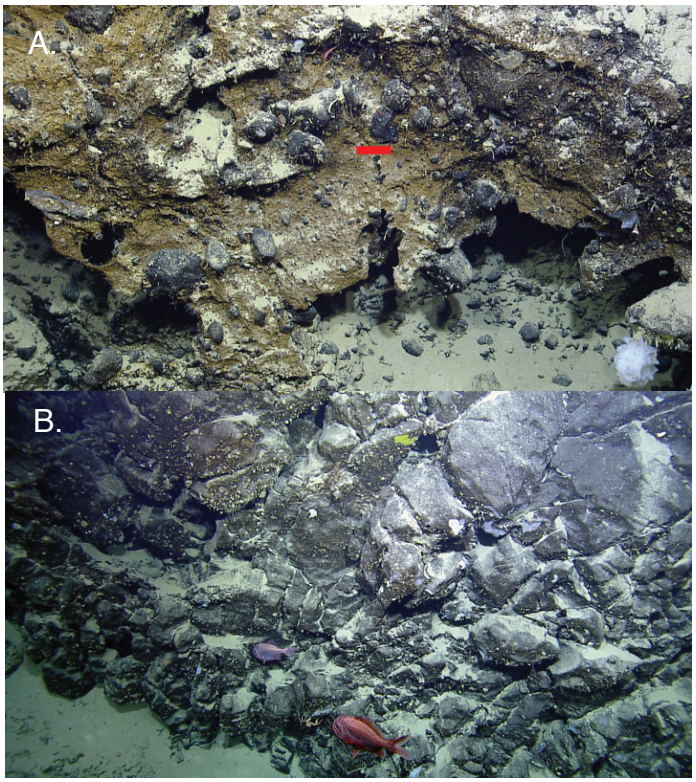
A.
B.

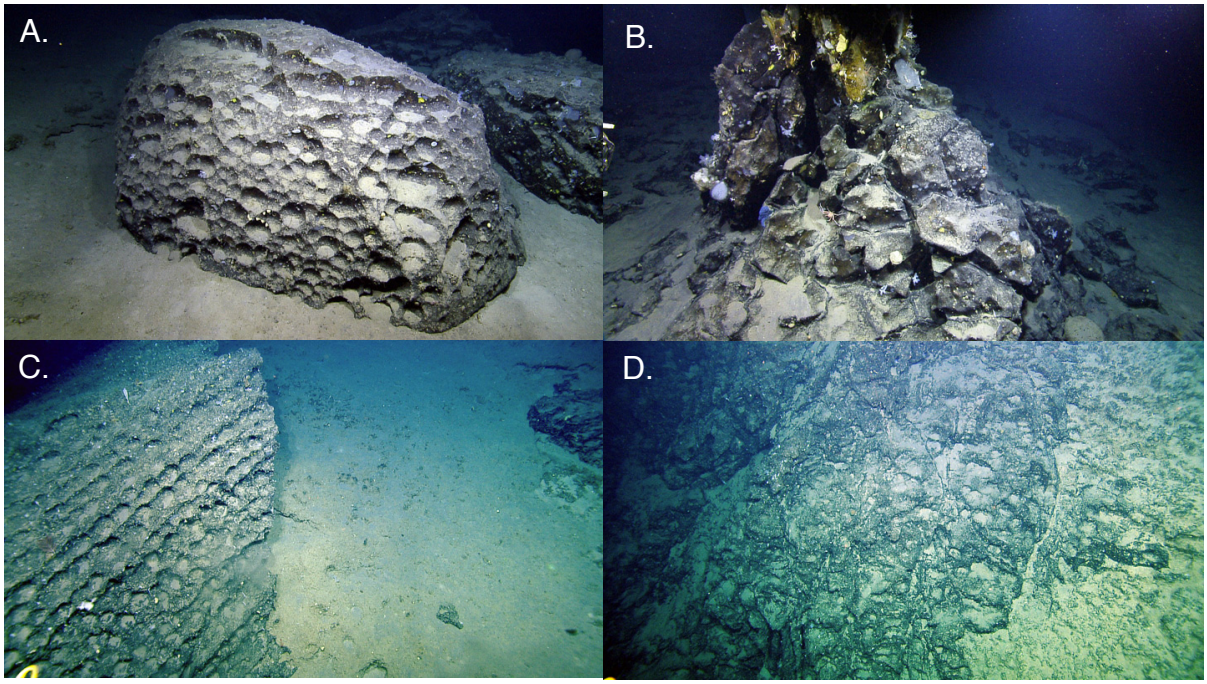
A.
B.
C.
D.

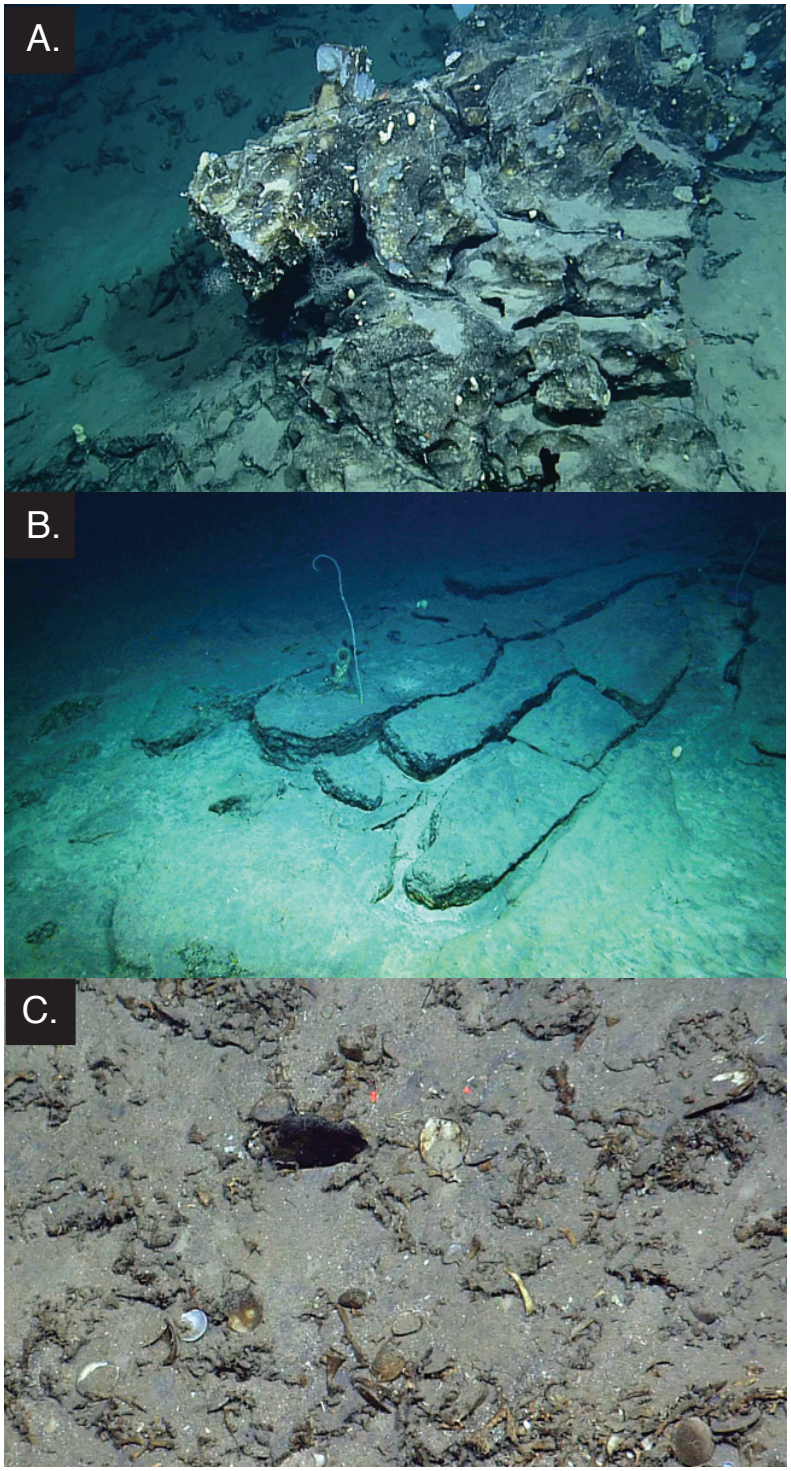
A.
B.
C.

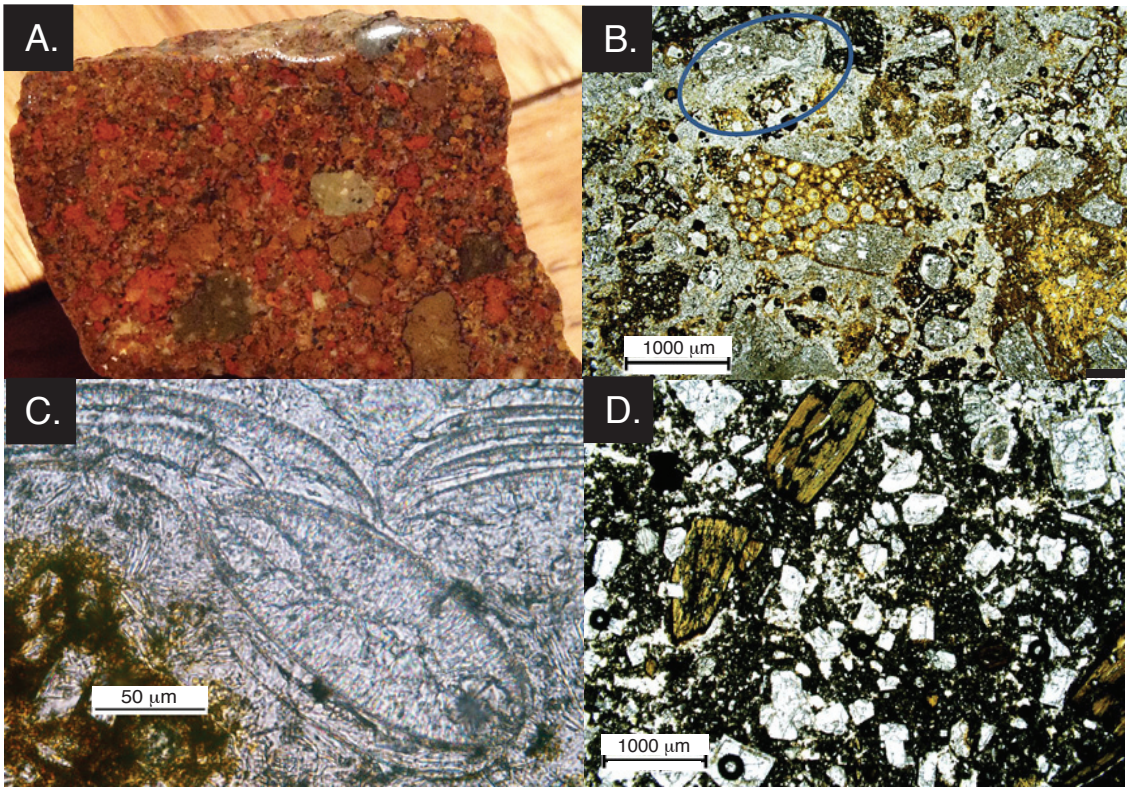
A.
B.
1000 μm
C.
50 μm
D.
1000 μm

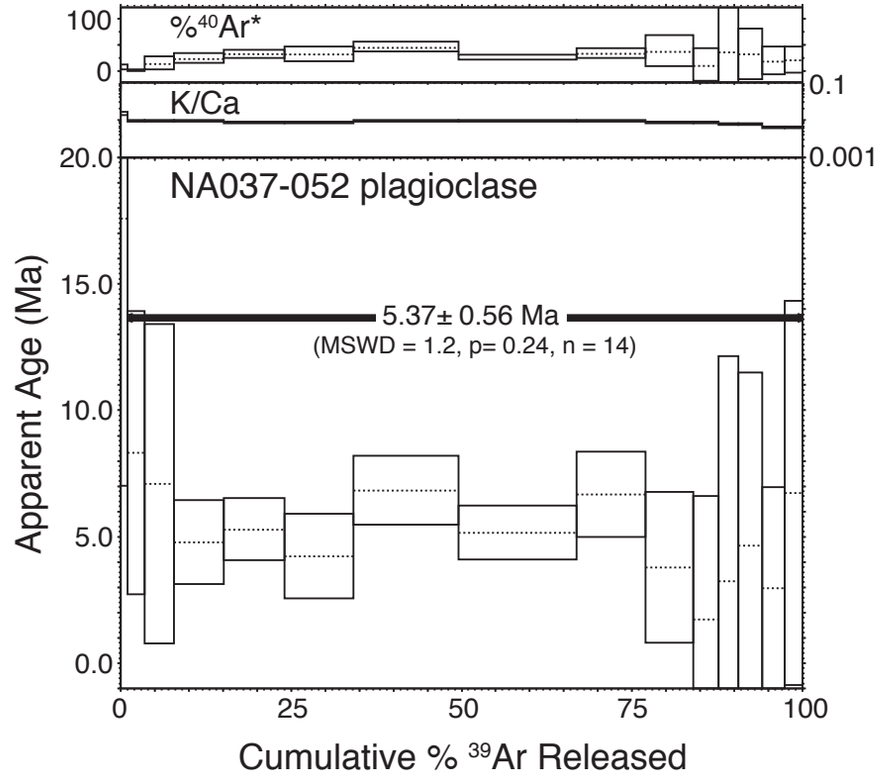
%40Ar*
K/Ca
NA037-052 plagioclase
5.37± 0.56 Ma
(MSWD = 1.2, p= 0.24, n = 14)
Apparent Age (Ma)
Cumulative % 39Ar Released

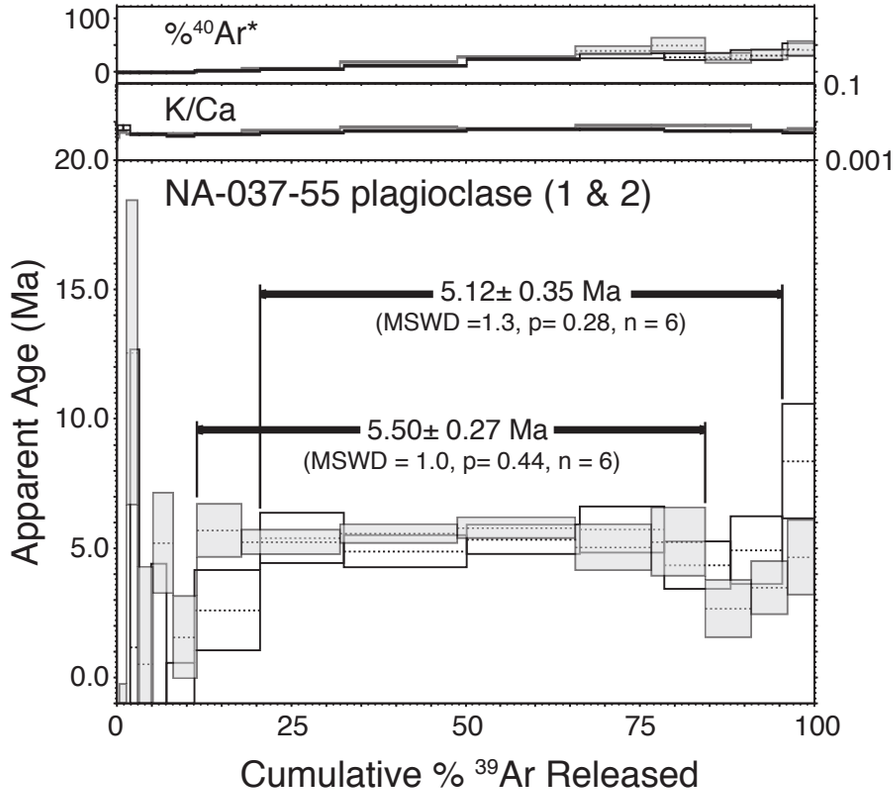
%40Ar*
K/Ca
NA-037-55 plagioclase (1 & 2)
5.12± 0.35 Ma
(MSWD =1.3, p= 0.28, n = 6)
5.50± 0.27 Ma
(MSWD = 1.0, p= 0.44, n = 6)
Apparent Age (Ma)
Cumulative % 39Ar Released

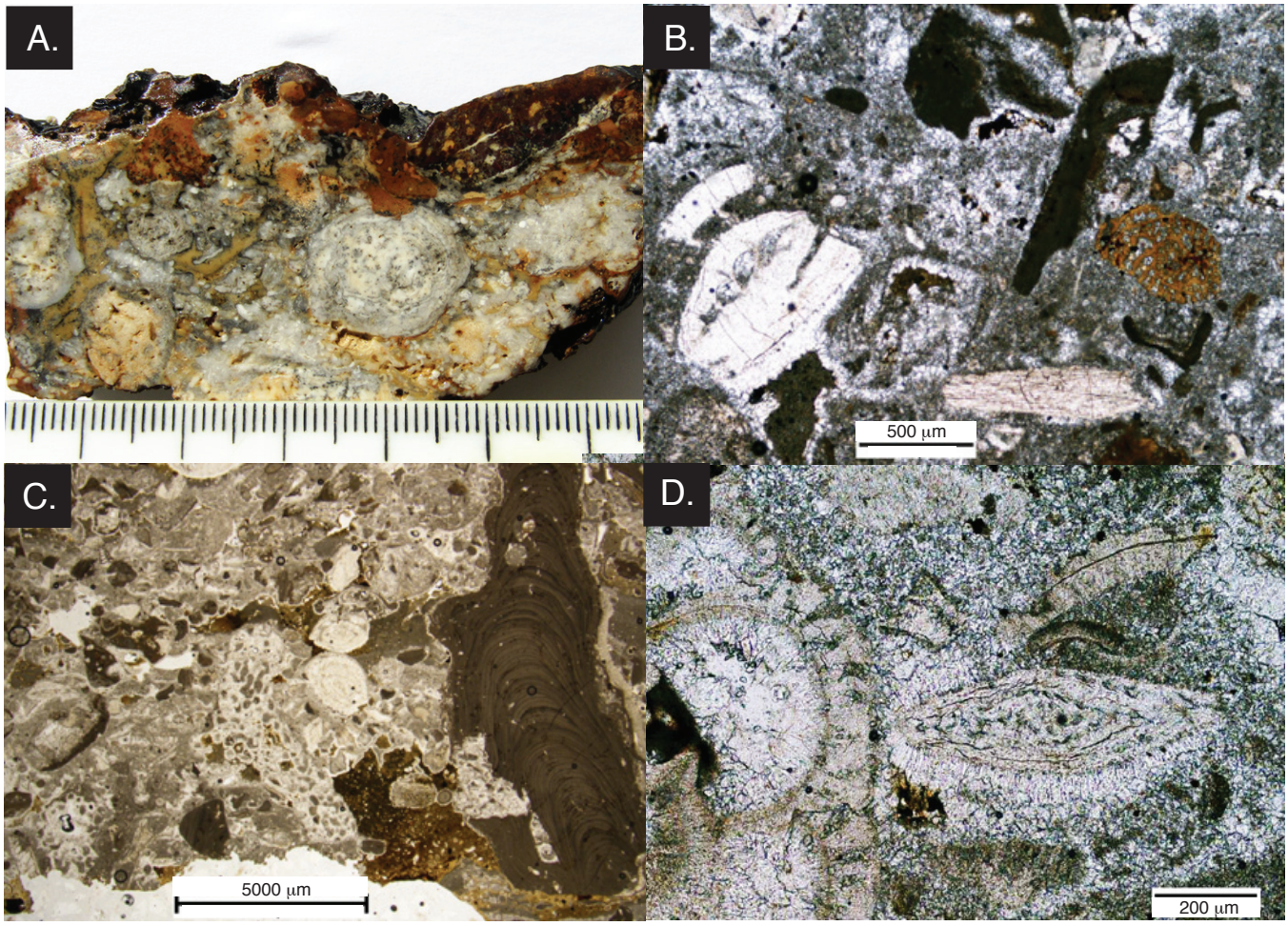
A.
B.
500 μm
C.
5000 μm
D.
200 μm

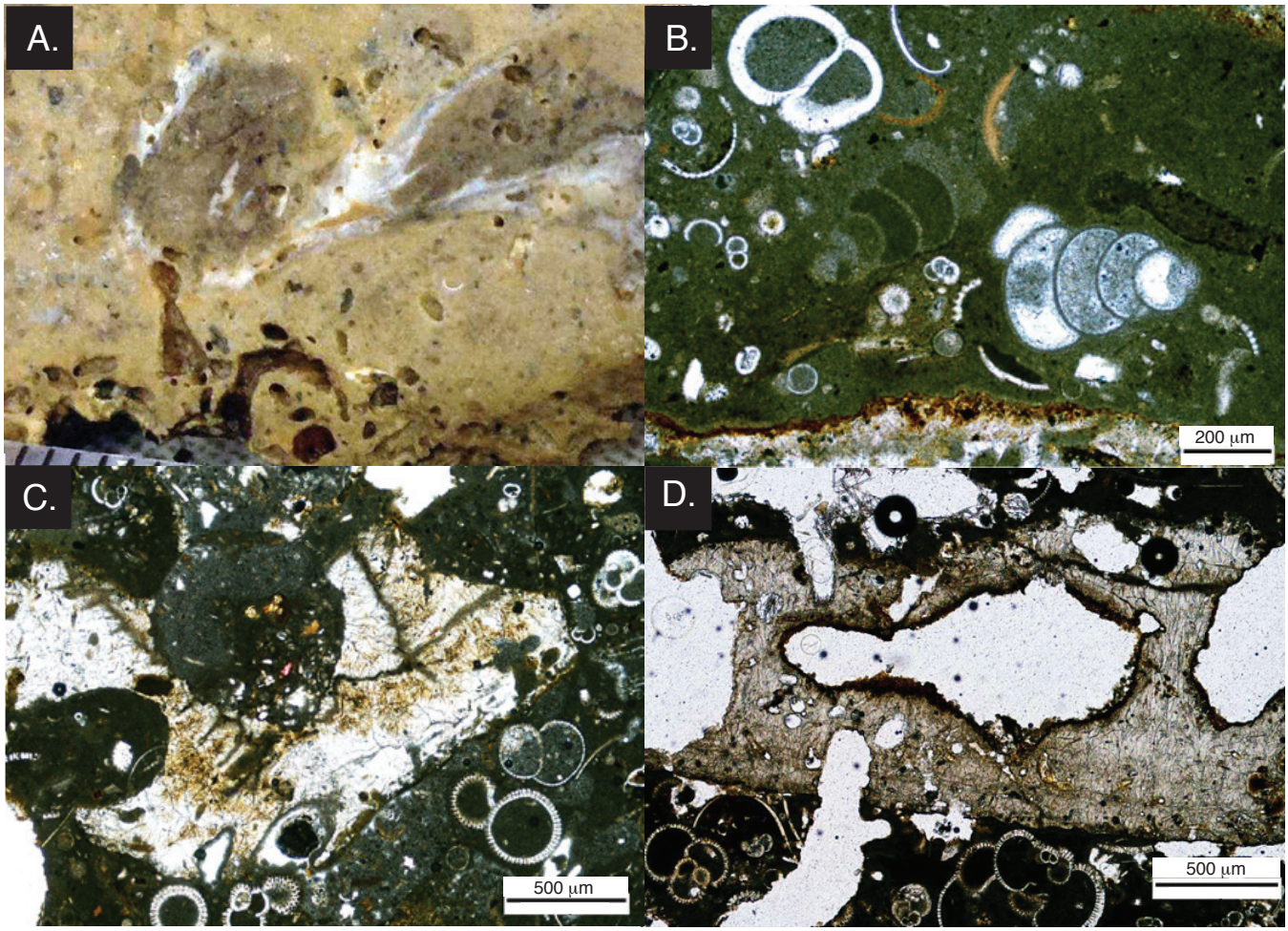
A.
B.
200 μm
C.
500 μm
D.
500 μm

Figure 12

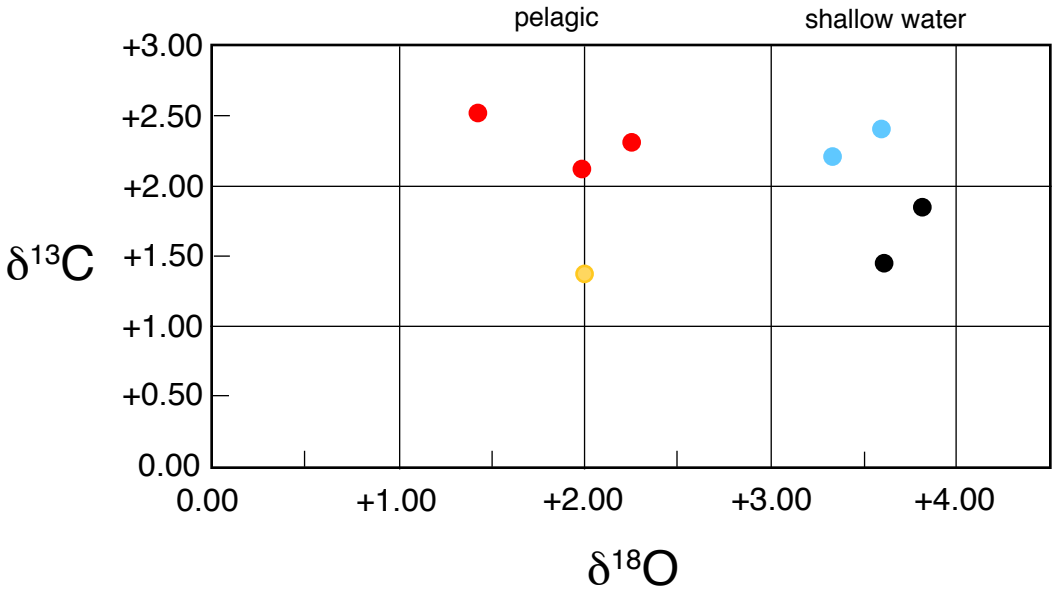
pelagic
shallow water
+3.00
+2.50
+2.00
+1.50
+1.00
+0.50
0.00
δ13C
0.00
+1.00
+2.00
+3.00
+4.00
δ18O

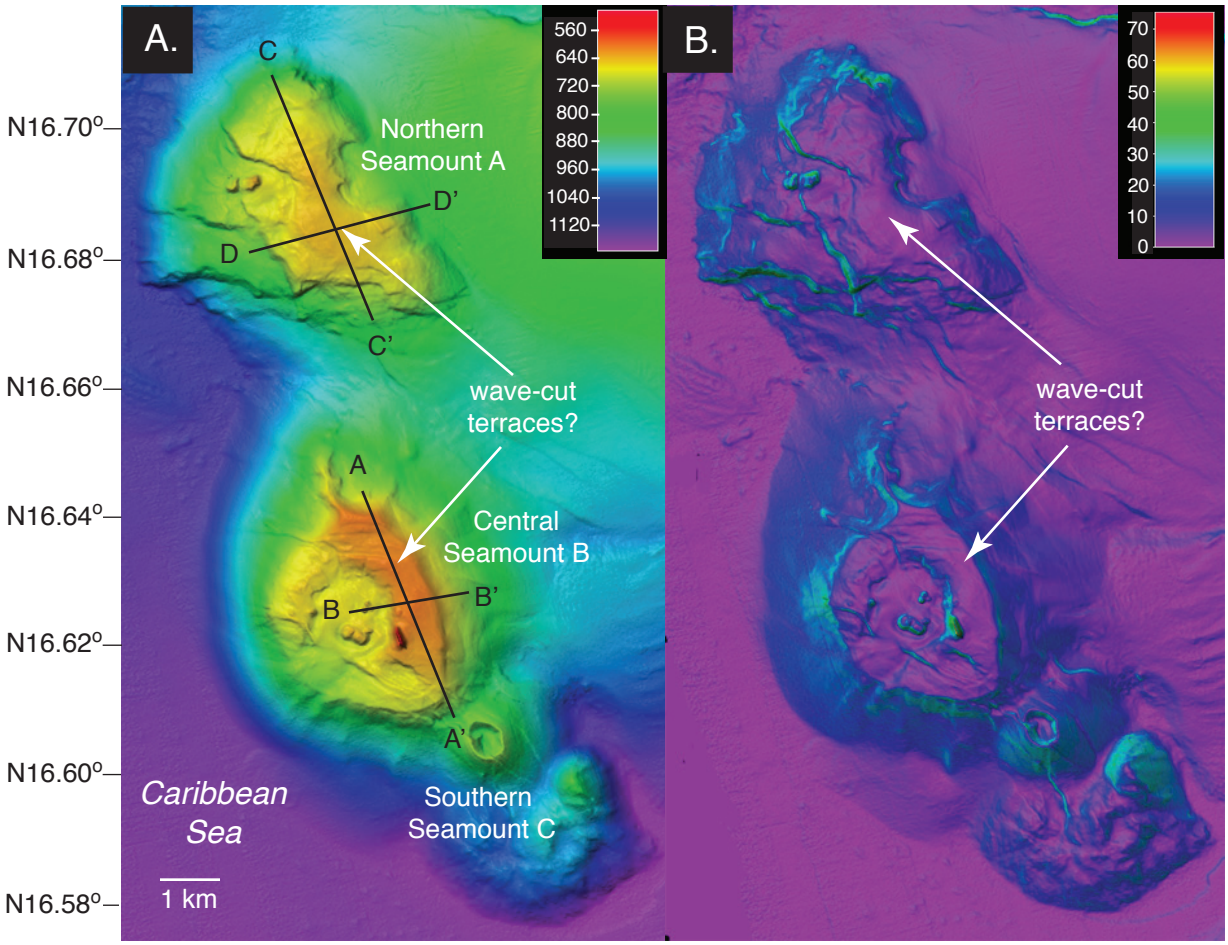
A.
B.
C
C'
D
D'
A
A'
B
B'
Northern
Seamount A
Central
Seamount B
Southern
Seamount C
wave-cut
terraces?
wave-cut
terraces?
Caribbean
Sea
1 km
560
640
720
800
880
960
1040
1120
70
60
50
40
30
20
10
0
N16.70°
N16.68°
N16.66°
N16.64°
N16.62°
N16.60°
N16.58°

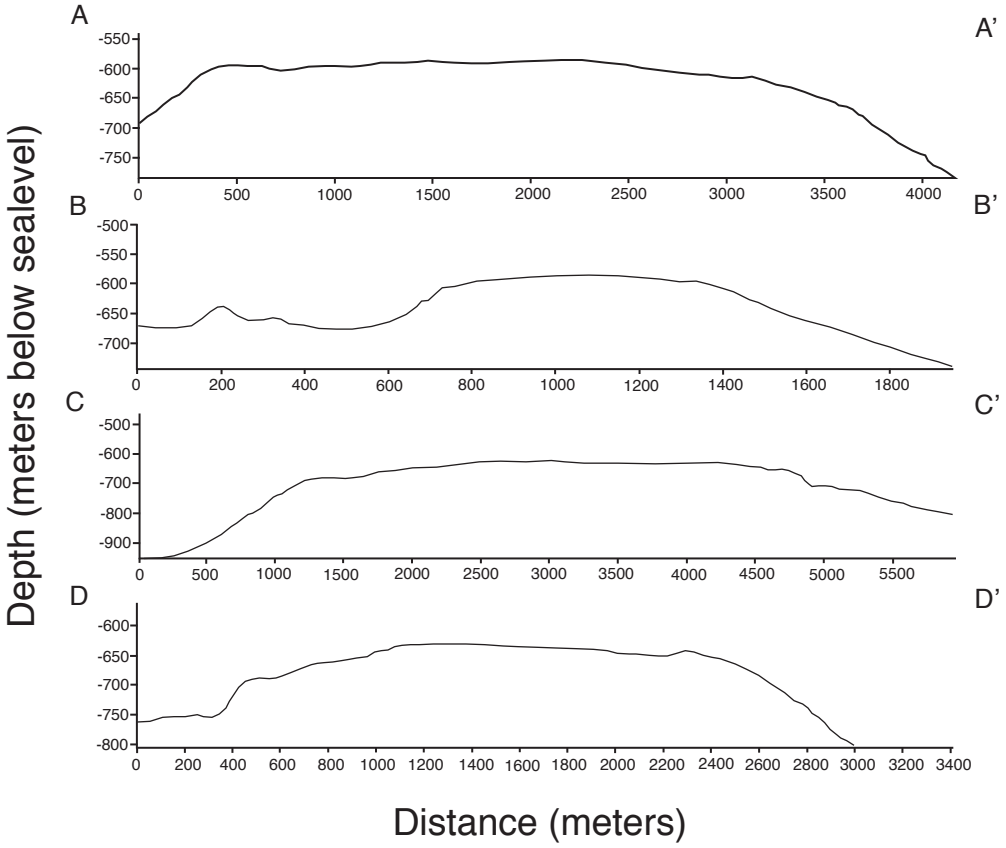
A
A'
-550
-600
-650
-700
-750
0
500
1000
1500
2000
2500
3000
3500
4000
B
B'
-500
-550
-600
-650
-700
0
200
400
600
800
1000
1200
1400
1600
1800
C
C'
-500
-600
-700
-800
-900
0
500
1000
1500
2000
2500
3000
3500
4000
4500
5000
5500
D
D'
-600
-650
-700
-750
-800
0
200
400
600
800
1000
1200
1400
1600
1800
2000
2200
2400
2600
2800
3000
3200
3400
Depth (meters below sealevel)
Distance (meters)

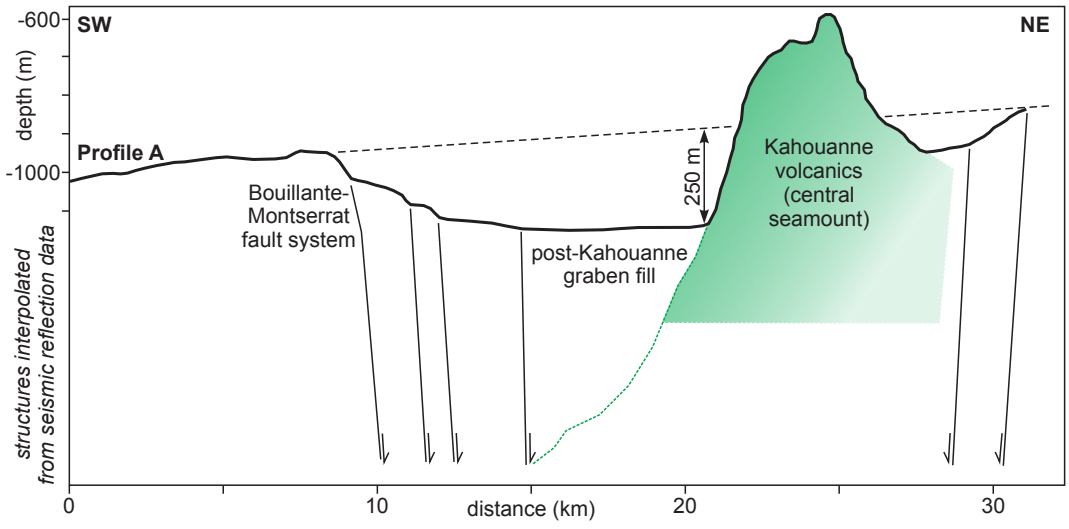
-600
-1000
depth (m)
SW
NE
Profile A
250 m
Kahouanne
volcanics
(central
seamount)
Bouillante-
Montserrat
fault system
post-Kahouanne
graben fill
structures interpolated
from seismic reflection data
0
10
distance (km)
20
30